Physics – Uspekhi **69** (1) 42 – 73 (2026)

INSTRUMENTS AND METHODS OF INVESTIGATION PACS numbers: **34.35. + a,** 68.49.Sf, 79.20.Rf

Surface analysis by low-energy ion scattering spectroscopy

A.B. Tolstoguzov, P.Yu. Babenko, A.N. Zinoviev

DOI: https://doi.org/10.3367/UFNe.2025.09.040043

Contents

Abstract. The physical processes underlying the technique that uses low-energy (0.5–5 keV) backscattered ions of noble gases (Low Energy Ion Scattering, LEIS) and its hardware implementation are reviewed. The specific features of LEIS surface diagnostics, including the interpretation of energy spectra, quantitative elemental analysis, and options for studying the surface structure, the particle–surface interaction potential, and the presence of clusters in solid solutions, are discussed. Software codes for computer modeling of ion–surface interaction processes are presented. The advantages of energy-mass analysis of scattered ions are considered; the application of ion scattering in state-of-the-art ion microscopes is discussed, and the scattering of noble gas ions in the hyperthermal energy range is examined. The main areas of LEIS application for the analysis of the surface and near-surface layers of various materials and devices are overviewed, and the prospects for further development of low-energy ion scattering spectroscopy are assessed.

A.B. Tolstoguzov [1, 2, 3, *], **P.Yu. Babenko** [4], **A.N. Zinoviev** [4]
[1] Utkin Ryazan State Radio Engineering University, ul. Gagarina 59/1, 390005 Ryazan, Russian Federation
[2] Zhuhai Tsinghua University Research Institute Innovation Center, 519000 Zhuhai, China
[3] Centre for Physics and Technological Research (CeFITec), Universidade Nova de Lisboa, 2829-516 Caparica, Portugal
[4] Ioffe Institute, Russian Academy of Sciences, ul. Politekhnicheskaya 26, 194021 St. Petersburg, Russian Federation
E-mail: [*] tolstoguzov52@mail.ru

Received 13 January 2025, revised 23 September 2025
Uspekhi Fizicheskikh Nauk **196** (1) 48 – 82 (2026)
Translated by M.Zh. Shmatikov

Keywords: surface diagnostics, ion scattering, neutralization, sputtering, fast ionized recoil atoms, energy-mass analysis, hyperthermal energy, ion microscopes

1. Introduction

Surface science, and particularly its applied fields, began to develop rapidly in the mid-1960s. This progress was based on the then-cutting-edge advances in emission electronics, solid-state physics, vacuum technology, and radioelectronics. It was driven by the pursuit to better fulfill the growing needs of manufacturers of semiconductor and microelectronic devices and thermionic emitters, and the development of new types of thin-film coatings and effective catalysts, and later, biomedical technologies. At the same time, the term 'surface diagnostics of surface analysis' emerged, and a set of physical methods appeared that allowed the elemental composition of the surface and subsurface layers to be analyzed and their structure and electronic properties to be determined under high and ultrahigh vacuum conditions. These methods were primarily based on the interaction of electrons, photons, and atomic particles (ions, neutral atoms, and molecules) with the surface. The useful signal was either the surface's 'response' to such interaction, such as by means of sputtering, or changes in the characteristics of the primary (probe) particles, primarily their energy, after interaction with the surface. Major international manufacturers of sophisticated analytical equipment, such as Varian, Perkin Elmer, Physical Electronics, and Thermo Fisher Scientific played a significant role in the development of surface diagnostic techniques. They managed to rapidly develop and deploy mass production of various systems, including multi functional ones.

This review focuses on ion scattering spectroscopy (ISS), a method based on the backscattering (reflection) of ions from surface atoms. It should be noted that this method has several names, which are used in both Russian and international (English-language) scientific publications. Following the maxim of the French philosopher and mathematician René Descartes: "Almost all controversy would be removed from among Philosophers, if they were always to agree as to the meaning of words" [1], we make an attempt to clarify and systematize the names of this method for further use in our review.

First and foremost, we note that, depending on the energy of the primary ions, ion scattering methods are divided into low-, medium-, and high-energy ion scattering. In the low-energy range — usually 0.5–5 keV — the primary name is Low Energy Ion Scattering (LEIS), sometimes LEISS (with Spectroscopy added) [2], i.e., low-energy ion scattering, which has recently been supplemented with the prefix HS (High Sensitive, HS-LEIS) [3] — a highly sensitive method of low-energy ion scattering. In the Russian-language scientific publications, the terms ion-scattering spectroscopy (ISS) (ionno-rasseivatel'naya spektroskopiya, IRS) [4], backscattered low-energy ion spectroscopy (BSLEIS) (spektroskopiya obratno rasseyannyh ionov nizkih energij, SORINE) [5], and slow ion scattering (LIS) (rassiyanie medlennyh ionov, RMI) [6] are used. Medium energy (50–500 keV) methods are called MEIS (Medium Energy Ion Scattering) [7, 8], and in Russian-language publications, MEISS (Medium Energy Ion Scattering Spectroscopy) (spektroskopiya rasseyaniya srednih energij, SRSE) [9]. Finally, scattering of high-energy ions (over 500 keV) is called in Russia Rutherford backscattering (RB) (rezerfordovskoe obratnoe rasseyanie, ROR) [10] and international, RBS (Rutherford Backscattering Spectrometry) [11]. Note that the energy ranges of the methods listed above may differ slightly among different authors.

Each of the aforementioned techniques has characteristics of its own related to the processes of ion interaction with the surface (scattering events), the interpretation of measurement results, and the hardware implementation. To justify the choice of energy ranges, a comparison of the velocities of primary ions and electrons in a solid is sometimes applied: LEIS — the primary ion velocity is lower than the electron velocity (elastic scattering predominates), MEIS — the ion velocity is approximately the same as the electron velocity (inelastic scattering), and RBS — the ion velocity is higher than the electron velocity (nuclear interactions).

We now specifically discuss the topic of this review. We do not touch the scattering of medium- and high-energy ions, but only consider low-energy ion scattering, using the abbreviation LEIS to denote this method. Moreover, we are primarily interested in the scattering of positive ions of inert (noble) gases, although scattering of alkali metal ions and active gases is also considered [12–16].

So, the main subject of our review is the elemental analysis of surface composition, including quantitative analysis by means of the LEIS method using not only light helium ions but also heavier neon and argon ions. We also discuss the potential for studying the chemical composition and crystallographic structure of surfaces using ion scattering and fast recoil atoms. In the section devoted to promising areas of LEIS development, we detail the implementation features and advantages of energy-mass analysis of scattered ions, and discuss the application of ion scattering in state-of-the-art ion microscopes. In our opinion, the scattering of noble gas ions in the hyperthermal energy range (below 100 eV) is of particular interest. In the application section, we discuss the results obtained in studies of nanoparticles and clusters, materials, and microelectronic devices, including their depth profiling and the feasibility of conducting chemical analysis based on measurements of oscillations in the signal intensity of scattered ions with variation of the energy of the primary ions. In addition to analyzing solids, LEIS is used to examine the surfaces of liquid media, which is also discussed in our review. All of the above issues have either not been considered at all in reviews and monographs on low-energy ion scattering known to us or received insufficient attention.

Brief historical background

The backscattering of low-energy ions by metal surface atoms as a result of binary elastic collisions (BECs), which is analogous to collisions of atomic particles in the gas phase, was first discovered in 1951 by Soviet physicists Arifov [17] and Eremeev [18]. The birth of ion scattering spectroscopy can be considered to be the study by Panin [19], who measured the energy spectra of secondary ions formed during the interaction of various positive primary ions, including ions of the inert gases He^+ and Ar^+ with energies of 7.5–80 keV, with the surfaces of molybdenum and beryllium targets. It should be noted that the term 'secondary ions' was later used exclusively to denote low-energy ions, formed during surface sputtering by ion beams and which provide information in secondary ion mass spectrometry (SIMS [20]).

In [19], the energy distributions of backscattered ions and ionized recoils were measured and interpreted using classical laws of conservation of momentum and energy of interacting particles. It was shown that the energy of such ions depends on that of the primary ions, the mass ratio of the primary ions to the surface atoms, and the angle through which the primary ions are scattered after impacting the surface atoms. The interpretation/decoding of the spectra of scattered ions and recoil atoms is discussed in detail in Section 2. Here, we note that, in [19], it was experimentally proven that the energy spectra of these ions are described by the laws of elastic collisions of hard balls (as in a game of billiards).

LEIS as a method for elemental analysis of the upper layer of surface atoms was first described in detail and tested by D.P. Smith [21–23], who reported the energy spectra of He^+ and Ne^+ ions with energies of 0.2–2 keV, scattered at an angle of 90° from the surface of various targets, including polycrystalline copper, gold, polar faces of CdS and ZnS crystals, and aluminum oxide. It was shown that these spectra, as in study [19], exhibit peaks of single binary elastic collisions of He^+ and Ne^+ ions with surface atoms of the corresponding targets. For comparison, the scattering spectra of 1.8-keV atomic and molecular hydrogen ions from an Au surface were measured. These differed from the similar He^+/Au scattering spectra by the presence of an intense background at energies lower than that of the single elastic scattering peak.

The measurements were carried out under ultrahigh vacuum conditions (10^{-8} Pa) using a 127° sector electrostatic cylindrical deflector (Hughes–Rozhansky capacitor) and an electron multiplier. The author of this review patented the equipment and method for analyzing the surface of solids using the LEIS method in 1969 [24], and his inventor's certificate was registered in the USSR.

Among the first studies using the LEIS method, one can also note experiments [25–27] conducted in the early 1970s at German and Dutch universities. The last quarter of the 20th century can be considered the 'golden age' for surface

analysis methods, including Auger Electron Spectroscopy (AES), X-ray Photoelectron Spectroscopy (XPS or Electron Spectroscopy for Chemical Analysis, ESCA), Low-Energy Electron Diffraction (LEED), the above-mentioned SIMS, and many others. Books on surface analysis methods were regularly published abroad (for example, [28–31]) and promptly translated into Russian. In the Soviet Union, research papers, original monographs, and reviews on surface analysis using various methods were also published (we only cite a few of them [32–35]), including ion scattering [4, 5, 36, 37]. Currently, the publication of monographs, reviews, and textbooks on surface physics and analysis actively continues (e.g., [38–40]).

Among the listed surface analysis methods, LEIS stands out for its minimal analyzed layer depth, i.e., sensitivity to the elemental composition of the upper surface layer, and the ability to quantitatively interpret the research results. The first measurements of scattered ion signal oscillations as a function of primary ion energy [41] gave hope that this method can be used to carry out chemical surface analysis, with LEIS at that time being considered one of the main competitors to XPS/ESCA. In terms of hardware, most LEIS systems were laboratory instruments, although major international companies had already begun manufacturing multifunctional spectrometers for surface diagnostics, which included low-energy ion scattering equipment. Typically, the core methods employed in such systems were AES and XPS. Optimal operating conditions were created for them, while LEIS remained a complementary technique. The basic concepts of LEIS and the main results of applied research conducted during this period are described in detail in [42], which, in addition to the previously mentioned publications from the USA, the Netherlands, and Germany, provides a review of studies conducted in the UK, Australia, Belgium, Japan, Argentina, and other countries.

The majority of LEIS research conducted in the USSR at that time was not covered in review [42] or other international publications on surface analysis. In the Russian scientific publications, the results of exploring ion scattering, mainly of a basic nature, conducted at universities and academic research centers (Moscow State University, Moscow Aviation Institute, Moscow Engineering Physics Institute, Leningrad Polytechnic Institute, Physical-Technical Institute, Research Institute of Nuclear Physics of Moscow State University, etc.), were published in [4, 8, 43, 44]. One should note the great contribution of V.E. Yurasova, an initiator and organizer of international conferences on ion surface interaction (ISI), the agenda of which included a section on ion scattering. Since 1971 and to the present day, these conferences have been held every two years in various cities of the USSR and Russia. The last (27th) conference, ISI-2025, was held at the end of August 2025 in Ryazan. V.E. Yurasova and her colleagues, D.S. Karpuzov, V.A. Eltekov, V.I. Shulga, et al., were among the first to apply computer modeling in conjunction with experimental studies to examine the angular and energy distributions of ions scattered from the surfaces of various single crystals, including in the temperature range of magnetic phase transitions [45].

Fairly scant information can be found in Russian scientific publications on ion scattering about the development of analytical equipment for LEIS and the results of applied research conducted on such equipment at the Research Technological Institute (NITI, Ryazan) from 1977 to 1993. This institute was a research center of the Ministry of Electronic Industry (USSR MEI), and the results of equipment development and most of the research conducted at this and MEI's other research institutes were published only in Russian in specialized industry publications distributed by the Central Research Institute Elektronika (see, for example, [5]). Some of these studies can be found in monograph [4].

The initiator of the work on LEIS and other surface diagnostic methods at NITI and a founder of this institute was G.N. Shuppe, a recognized international authority in the field of emission (cathode) electronics (see, for example, the monographic review by H. Kawano [46] on the electron work function, which contains 18 references to the studies of G.N. Shuppe and his collaborators). The first studies using the LEIS method conducted at NITI in the late 1970s and early 1980s were focused on examining the operating mechanisms of effective thermionic cathodes [47–49] and adsorption/segregation processes on the surface of metal alloys [50]. Subsequently, work on LEIS was continued at NITI in S.S. Volkov's laboratory; their results are discussed in Section 4. An important output of their activities was the creation by the NITI team under the leadership of A.G. Denisov, the NITI director, of a prototype of the UAE.OPR-5-007 installation for studying the surface of solids using AES-LEIS methods. In the early 1980s, this installation was presented at the international scientific and technical exhibition held at the Moscow-based Sokolniki exhibition center.

In the early 1990s, NITI, like most industrial research institutes in the USSR, was closed. However, as the German poet Wilhelm Busch noted: ''Einszweidrei, im Sauseschritt Lüft die Zeit; wir laufen mit'' (''One, two, three, at breakneck speed time runs on; and we keep pace with it'') [51]. Abroad, LEIS continued to be developed and improved, primarily through the efforts of H.H. Brongersma and his colleagues from the Eindhoven University of Technology (Netherlands). Brongersma also headed Calipso B.V., a company which carried out analytical studies using the LEIS method and provided services for the installation of equipment for this method. The main achievements in this area, primarily concerning neutralization of scattered ions and, based on this, a quantitative approach to the assessment of the elemental composition of the surface using the LEIS method, are described in detail in review [2]. A monographic review [52] is also devoted to the problems of neutralization and charge exchange processes of slow inert gas ions interacting with solid surfaces.

It should be noted that, at that time, XPS, SIMS, and rapidly developing scanning probe microscopy methods (see, for example, [53] and the references cited therein) were gaining leadership positions in surface diagnostics. The dominance of these methods was reinforced by the mass production of equipment with the corresponding methodological and software support, which the LEIS method lacked. The era of 'homemade' laboratory instruments for surface diagnostics was approaching its end.

An important step that kept LEIS afloat was Brongersma's collaboration with the German company IONTOF [54], a leading manufacturer of TOF-SIMS and Orbitrap SIMS secondary ion mass spectrometers. A result of this collaboration was the development and industrial production of the Qtac100 (Quantitative Top Atomic Layer Characterization) module, which implemented a highly sensitive low-energy ion scattering method, called HS-LEIS, as mentioned earlier [3]. This module, the design of which is discussed in detail in [55], could be equipped with TOF-SIMS setups, and it could also

be operated as a stand-alone device. Enhanced elemental sensitivity was achieved through the use of a double toroidal energy analyzer and time-of-flight mass filtration of scattered and sputtered secondary ions. The advantages of HS-LEIS are discussed in reviews [55, 56], the most recent of which, published in 2024, is a practical guide to the interpretation of LEIS spectra, primarily for users of the Qtac100 module. Currently, most LEIS studies are carried out on such setups. This 'monopolization,' which has both positive and negative aspects, is also characteristic of other surface diagnostic methods, such as SIMS.

In parallel with the elemental analysis of surface composition using LEIS, crystallographic structural analysis of surfaces was developed using low-energy ions (e.g., [42, 57]). In this area, the significant contribution of Soviet researchers should be noted (e.g., [8, 43, 44, 58, 59]). Firsov's potential, his proposed solution to the inverse scattering problem, and his contribution to particle stopping theory won worldwide recognition. The work of V.E. Yurasova and colleagues was directly related to the discovery of ion scattering anisotropy, trapping, and long-term motion of ions in surface semichannels [60–63]. Scattering on atomic chains was theoretically studied and numerically modeled by Yu.V. Martynenko [64].

2. Theoretical foundations of LEIS method

The elemental analysis of solid surfaces using the LEIS method is based on the kinematic and dynamic laws governing the interaction of two isolated atomic particles (regardless of their charge state), which can be considered in a model of binary elastic collisions of atomic particles. This has been experimentally confirmed by many authors (see, for example, the studies cited in Section 1, primarily Panin's publication [19]). A peak is observed in the energy spectrum of scattered particles, corresponding to the laws of conservation of momentum and energy in elastic scattering. In many publications on ion scattering, this peak is referred to as a surface peak.

Figure 1a shows the scattering spectra of He^+ with primary energies of 1, 2, and 3 keV at an angle $\theta = 147°$ from the surface of polycrystalline tungsten (k_{an} is the coefficient of the energy analyzer, which allows the sweep voltage U supplied to the deflection plates of the analyzer to be converted into the energy of the analyzed ions E_1). The data are taken from the *Atlas of the Spectra of Backscattered Ions of Inert Gases* [65], which also presents the spectra for helium and neon ions with energies of 1, 2, and 3 keV, scattered from the surface of pure metals Ni, Cu, W, Pb and semiconductor materials Si and GaAs. The measurements were carried out using the 09IOS-1-009 setup. Figure 1a for $E_0 = 3$ keV shows a pronounced, extended, flat peak (bump) from multiply scattered and re-ionized ions at energies lower than the surface peak. This peak may mask scattering peaks from other atoms present on the sample surface whose masses are, however, lower than that of W atoms. Decreasing the energy of the primary He^+ ions (see insets in Fig. 1a) reduces the intensity of the bump, which almost completely disappears at $E_0 = 1$ keV. For primary Ne^+ ions, even with an energy of 3 keV (Fig. 1b), the background intensity is minimal.

As the ion energy decreases, the depth of penetration of the beam particles into the target decreases, and, consequently, the background component in the spectrum decreases, i.e., the contrast of the observed surface peak increases. Variations in the peak-to-substrate ratio are displayed in Fig. 1a. Therefore, the use of low-energy ions for surface analysis is preferable.

2.1 Basic kinematic formulas

Figure 2 schematically shows the interaction of a primary ion with mass M_0 and velocity v_0 (kinetic energy E_0) moving at an angle β to the plane of the target surface with a target atom with mass M located in the uppermost (visible) surface layer. Assuming that the period of the atom's thermal oscillations is much longer than the particle interaction time, this atom can be considered at rest at the moment of collision. As a result of this interaction, the primary ion scatters in the laboratory coordinate system at an angle θ relative to the direction of its initial motion, losing part of its kinetic energy, which becomes equal to E_1. Consequently, the velocity vector changes its direction and magnitude, which is now equal to v_1. A conventionally stationary target atom M, called a fast recoil atom, begins to move with a velocity v_2 at an angle ψ relative to the direction of the initial motion of the incident ion, acquiring kinetic energy E_2 as a result of the collision.

Using the classical laws of conservation of energy and momentum of interacting particles and ignoring inelastic energy losses Q of the incident ion ($Q/E_0 \ll 1$), we obtain well-known relations for the energies of the scattered ion E_1

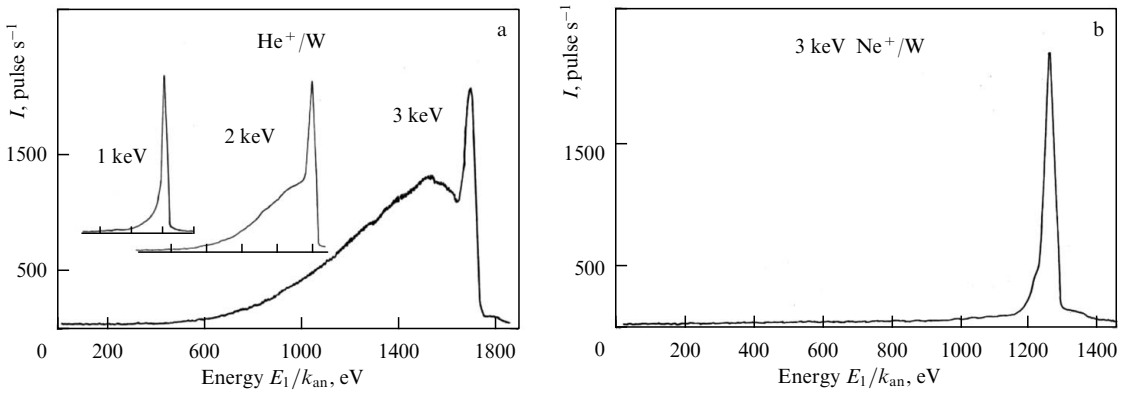

Figure 1. Energy spectra of He^+ ions with primary energies of 1, 2, and 3 keV (a) and Ne^+ ions with energy of 3 keV (b), scattered at angle $\theta = 147°$ from tungsten surface ($k_{an} = 0.64$) [65].

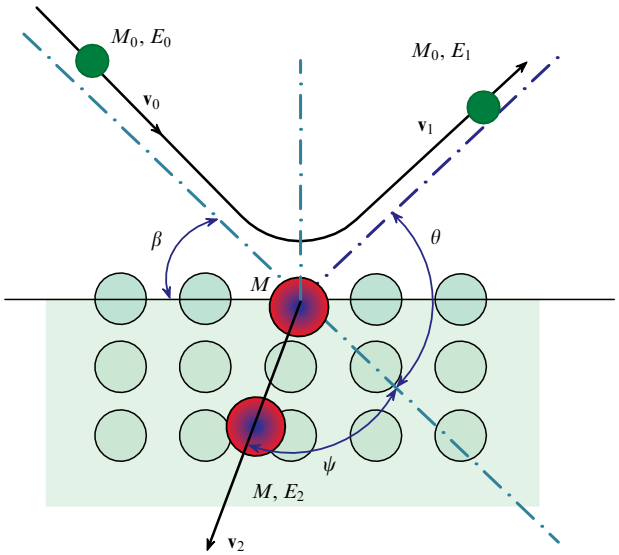

Figure 2. Schematic diagram of elementary scattering event.

and the recoil atom E_2:

$$E_1 = \left(\frac{\cos\theta \pm \sqrt{\alpha^2 - \sin^2\theta}}{1+\alpha}\right)^2 E_0 = K_1 E_0\,, \tag{1}$$

$$E_2 = \frac{4\alpha\cos^2\psi}{(1+\alpha)^2}\,E_0 = K_2 E_0\,, \tag{2}$$

where $\alpha = M/M_0$ is the relative mass, i.e., the ratio of the masses of the target atom and the primary ion, and K_1 and K_2 are the kinematic factors for the scattered ion and the recoil atom, respectively.

If inelastic energy losses Q are not disregarded, these formulas take the form [66]

$$E_1 = E_0\left(\frac{\cos\theta + \sqrt{\alpha^2 - \sin^2\theta - \alpha(1+\alpha)Q/E_0}}{1+\alpha}\right)^2, \tag{3}$$

or

$$\frac{Q}{E_0} = 1 - \mu - (1+\mu)\,\frac{E_1}{E_0} + 2\mu\sqrt{\frac{E_1}{E_0}}\,\cos\theta\,, \tag{4}$$

where $\mu = \alpha^{-1}$.

For $\alpha \geqslant 1$, i.e., when the mass of the surface atom is equal to or larger than that of a primary ion, only the plus sign remains after the cosine in Eqn (1), and the scattering angle θ can vary from zero to 180°. In this case, the mass of atom M can be calculated using the formula

$$M = M_0\,\frac{1 + E_1/E_0 - 2\cos\theta\sqrt{E_1/E_0}}{1 - E_1/E_0}\,. \tag{5}$$

If $\alpha < 1$, Eqn (1) retains its ambiguity, and the scattering angle cannot be greater than

$$\theta_{\max} = \arcsin\alpha\,. \tag{6}$$

An exact solution to the problem of elastic collisions of two particles using scattering and time integrals can be found, for example, in [67].

We emphasize that, for $\alpha < 1$, two values of energy E_1 are possible, while for $\alpha \geqslant 1$, only one value of the energy of backscattered ions is allowed. From a physical perspective, the existence of two possible energies of a primary ion forward-scattered at the same angle θ from a lighter surface atom implies the existence of two allowed impact parameters for the collision of these particles (see, for example, [4, 67]). It should be noted that, to our knowledge, experimental spectra with two peaks corresponding to such a collision have not been reported in publications. The formulas presented also show that, as the scattering angle decreases and the relative mass increases, the energy loss of the primary ion after scattering from the corresponding surface atom decreases.

Using Eqn (5), we can determine the mass spectral resolution of the LEIS method, i.e., mass interval $\Delta M = M_2 - M_1$, within which scattering peaks from surface atoms with masses M_2 and M_1 are separated at a given level of maximum intensity of these peaks:

$$\Delta M = \left[\frac{1-\alpha^2}{\alpha(\alpha\cos\theta - \sqrt{\alpha^2 - \sin^2\theta})}\right] \times \left[\frac{\sqrt{\alpha^2 - \sin^2\theta}}{2}\left(\frac{\Delta E}{E}\right)_a + \sin\theta\,\Delta\theta\right], \tag{7}$$

where $(\Delta E/E)_a$ is the relative energy resolution of the analyzer at a given level of maximum intensity of the peaks, and $\Delta\theta$ is the range of permissible scattering angles, which is determined by the dimensions of the input aperture of the energy analyzer in the scattering plane.

Calculations using Eqn (7) for primary ions $^4He^+$, $^{20}Ne^+$, and $^{40}Ar^+$ with typical characteristics of LEIS spectrometers ($\theta = 120°$, $\Delta\theta = 1.5°$, $(\Delta E/E)_a = 0.03$) show that the mass resolution $\Delta M = 2$ amu can be achieved for primary ions $^4He^+$ in the range of surface atom masses of 5–26 amu; for $^{20}Ne^+$, in the range of 21–55 amu, and for $^{40}Ar^+$, in the range of 41–78 amu. Thus, when using $^4He^+$ ions, separating the peaks from aluminum ($M \cong 27$ amu) and silicon ($M \cong 28$ amu) atoms in the scattering spectra at a level of 10% of the maximum intensity of these peaks is a challenging task, but it can be solved using $^{20}Ne^+$ primary ions. However, in this case, a more significant contribution from sputtered secondary ions should be expected, the suppression of which requires the energy-mass analysis mode for scattered and sputtered ions.

In principle, the energy spectra of backscattered ions should be linear, but various instrumental and physical factors transform them into peaks, the shape and width of which, at least at a level of 50% of the maximum signal intensity (FWHM), are primarily determined by the hardware function of the energy analyzer. Other hardware factors include the angle of entry into the analyzer and the energy spread of the primary ions and the angles of incidence. The influence of these factors on scattered ion peaks is discussed in Section 3 devoted to LEIS hardware implementation.

2.2 Quantitative elemental analysis by LEIS method

By measuring the scattered ion current I_i, one can determine the surface concentration of atoms N_i from which these ions were scattered:

$$I_i = I_0 N_i R_i \eta_i A\,, \tag{8}$$

where I_0 is the primary ion current pertaining to the region of the energy analyzer in which scattered ions are collected, R_i is a coefficient accounting for surface roughness and

shadowing of the analyzed ith type atoms by neighboring atoms, η_i is the elemental sensitivity, or ion yield, and A is a hardware factor.

The last two coefficients in Eqn (8) require further explanation. The elemental sensitivity for atoms of the ith type is defined as

$$\eta_i = P_i^+ \frac{\mathrm{d}\sigma_i}{\mathrm{d}\Omega}\,, \tag{9}$$

where P_i^+ is the ion-survival probability that primary ions scattered from atoms of the ith type save their charge state, and $\mathrm{d}\sigma_i/\mathrm{d}\Omega$ is the differential scattering cross section, i.e., the ratio of the number of particles scattered per unit time into an element of solid angle $\mathrm{d}\Omega$ to the primary particle flux density.

The hardware factor can be represented as

$$A = TD\,\Delta\Omega\,, \tag{10}$$

where T is the transmittance of the energy analyzer, i.e., the ratio of the number of scattered ions at the analyzer input and output, D is the detector's efficiency for scattered ions, and $\Delta\Omega$ is the analyzer's solid entrance angle (acceptance).

To carry out quantitative analysis using Eqn (8), it is first necessary to know the elemental sensitivity, which is determined either theoretically or experimentally using calibration samples. The first approach is rarely used in LEIS surface diagnostics due to the difficulties in calculating the differential scattering cross section and, especially, determining the probability that scattered ions preserve their charge.

In an elementary scattering event, shown in Fig. 2, two particles interact; in practice, however, multiple primary ions interact with multiple surface atoms and are scattered at multiple angles, and the scattering cross section $\sigma(\theta)$ indicates how many particles are scattered at a given angle θ. In a laboratory coordinate system, the scattering cross section can be represented as [4, 67]

$$\sigma(\theta) \equiv \frac{\mathrm{d}\sigma}{\mathrm{d}\Omega} = \frac{p}{\sin\theta}\left|\frac{\mathrm{d}p}{\mathrm{d}\theta}\right|, \tag{11}$$

where p is the impact parameter, i.e., the perpendicular distance from the line along which the primary particle moves to the center of the interaction potential field $U(R)$ of this particle with a surface atom.

Equation (11) shows that the scattering cross section is uniquely determined by the interaction potential $U(R)$. The LEIS method primarily utilizes various approximations of the screened Coulomb potential, taking into account the screening of the nuclei of interacting particles by electron shells and the nature of the field perturbations during collisions of these particles [4, 8, 68–71].

The potentials most suitable in the range of primary ion energies of 0.1–5 keV are Ziegler–Biersack–Littmark (ZBL) [72], Zinoviev [73], and KrC [74], which agree quite well with each other in the specified collision energy range (Fig. 3). We also note the good agreement between these potentials and experimental data on ion scattering in gases and calculations in the density functional approximation [75]. The screened Coulomb potential in the Molière approximation [76], proposed in 1949, has a convenient functional form and is often used with a screening length adjustment. The empirical Born–Mayer potential is sometimes used [77, 78]. Tables of differential scattering cross sections calculated

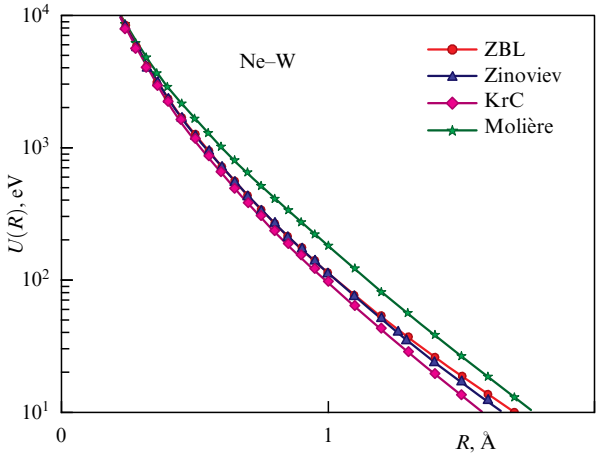

Figure 3. Interatomic interaction potential $U(R)$ for Ne/W system as function of internuclear distance R. ZBL [72], Zinoviev [73], KrC [74], and Molière [76] potentials are shown.

using the ZBL potential are presented in the appendix to monograph [4].

To summarize, for all interaction potentials, the scattering cross sections decrease monotonically with increasing primary ion energy and scattering angle. This reflects the fact that, with increasing energy and scattering angle, primary ions penetrate deeper into the atomic shells and, consequently, are subject to a greater extent to the effective nuclear charge of these atoms. With increasing relative mass α, i.e., with increasing surface atom mass M, the $\sigma(\theta)$ values also increase.

2.2.1 Charge fraction of scattered ions and today's achievements in its calculations. The most challenging aspect is determining the ion-survival probability (charge fraction) of scattered ions, P^+. It should be noted that, when scattering noble gas ions in the LEIS method, the P^+ value can at best reach a few percent, i.e., the overwhelming majority of primary ions are neutralized upon scattering from surface atoms. For ions that penetrate the target deeper than the surface layer, the probability of charge preservation is even lower, and if they undergo re-ionization, they contribute to the tail of re-ionized ions rather than to the surface peak. This explains the unique surface sensitivity of LEIS, which is the main advantage of this method, and also one of its main drawbacks — low elemental sensitivity.

The term 're-ionization' should be clarified. Some ions that penetrate deep into the target and are reflected there by located atoms deeper than the visible surface layer can be neutralized, losing some of their energy due to inelastic interactions with atoms and electrons, and then re-ionize as a result of head-on collisions with target atoms [2, 79, 80]. The physical processes responsible for re-ionization are complex and diverse, and re-neutralization of ions (collision-induced re-ionization and neutralization) can also occur alongside re-ionization.

The theory of neutralization of inert gas ions was initially developed in application to the phenomena of potential ion-electron emission and ion-neutralization spectroscopy, primarily for zero and near-zero energies of primary ions (see, for example, [81–83] and the references therein). The processes shown in Fig. 4 [84] were considered the main mechanisms of neutralization and charge exchange.

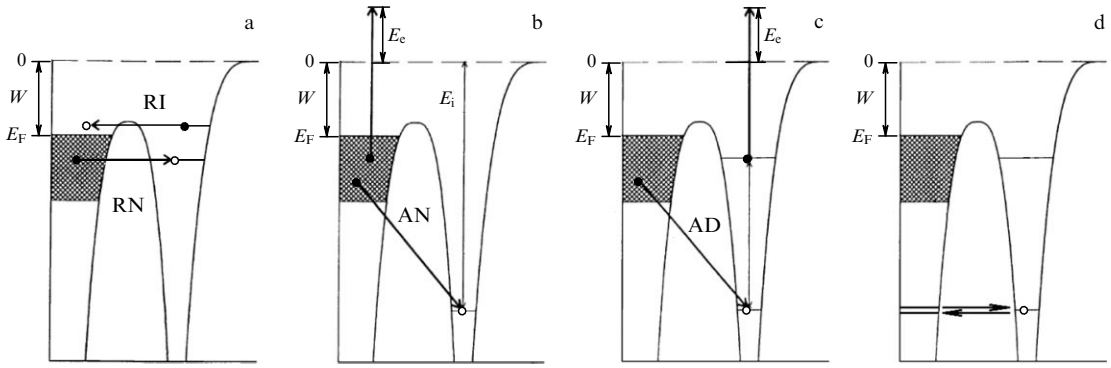

Figure 4. Various types of electron exchange: (a) resonant capture (RN — resonant neutralization, RI — resonant ionization), (b) Auger neutralization (AN), (c) Auger de-excitation (AD), (d) quasi-resonant exchange with deep level. Here, E_F is electron energy at Fermi level, W is electron work function, E_i is ionization energy, and E_e is electron energy in vacuum (after escaping from solid) [84].

The processes shown in Fig. 4 are briefly explained below.

(1) Resonant electron transition (resonant ionization and neutralization, Fig. 4a): electron exchange with the conduction band occurs with conservation of electron energy. The equilibrium charge state of an atomic particle during resonant electron exchange with metals is formed at characteristic distances of 5–10 au [1] from the surface.

(2) Auger neutralization (Fig. 4b) occurs through the transition of an electron from the conduction band or weakly bound level of the target atom to a deeper level of the ion, resulting in its neutralization. The energy released during the Auger process is transferred to another electron. The most common process is Auger electron capture by a positive ion (Auger neutralization).

(3) Auger relaxation (Auger deexcitation, Fig. 4c) of an excited neutral atom occurs at a characteristic distance of 2–4 au from the surface.

(4) Quasi-resonant electron exchange (Fig. 4d) with a deep (bound) level is realized for certain combinations of metals (Pb, Au) and noble gas ions (He^+, Ne^+).

(5) Nonresonant electron transitions occur via an electron transition with a change in electron energy. The probability of nonresonant transitions is low.

If Auger neutralization or resonant exchange dominates, the ion-survival probability for a scattered particle can be represented as

$$P^+ = \exp\left(-\frac{v_c}{v}\right), \qquad (12)$$

where v_c is the characteristic velocity (neutralization constant), which depends on the primary ion/surface combination and other experimental conditions, and $1/v = 1/v_{in} + 1/v_f$ is the reciprocal total velocity of the particle as it approaches the surface ($1/v_{in}$) and departs from it ($1/v_f$), i.e., during the final part of its trajectory.

In essence, the coefficient $1/v$ indicates the time the particle spent near the surface. It is recommended to use either the perpendicular component of the velocity [85] or the total velocity [86] as the velocities in Eqn (12), but in general the prevailing opinion is that the perpendicular component is better suited to describing the charge preservation processes in scattered ions in the LEIS method [2]. Some authors, for example [87], in studying the angular dependences of ion scattering, came to a conclusion that v_c in formula (12) is not a constant value, but depends on the angles of incidence β and scattering θ. However, a satisfactory explanation for this phenomenon has not been proposed.

In [88], an original method was developed to determine the characteristic velocity during scattering of helium ions from the surface of a boron target. This method consists of using two isotopes, $^3He^+$ and $^4He^+$, as primary ions. At the same energy, they have different velocities, i.e., different P^+ values, but the same characteristic velocity v_c. The target was irradiated with helium isotopes sequentially, while the hardware factor and target properties remained unchanged. The method was called the "two-isotope surface composition technique." Later, a similar method, but using a larger number of Kr^+ isotopes and in the energy-mass analysis mode of scattered ions, was applied in [89] to determine v_c for a niobium target. In Section 6.1, devoted to the energy-mass analysis of scattered ions, we consider the advantages of this approach compared to energy analysis alone, including when studying the neutralization processes of scattered ions [90]. In general, for primary helium ions scattered from various targets, it was found that the values of v_c are in the range of 10^5–10^6 m s^{-1}. For heavier primary ions, including Ne^+, the data are quite contradictory, and the range of v_c values is much greater (see, for example, [91–94]).

The development of a theory of neutralization and charge exchange for slow inert gas ions interacting with solid surfaces, the foundations of which were laid back in the 1950s to 1970s, continues to attract the attention of researchers. For a more in-depth understanding of these processes, we recommend the review by Brongersma et al. on surface composition analysis using the LEIS method [2], the review by H. Winter [84], the review by R.C. Monreal [52] on Auger neutralization and ionization processes (the work was funded by the Spanish Ministry of Science and Innovation under the FIS2011-26516 project), and the review by Gainullin [6], recently published in *Physics Uspekhi*, which summarizes the current experimental and theoretical knowledge on resonant electron exchange during scattering of slow ions from metal surfaces. Unfortunately, at present, based on theoretical concepts of neutralization/charge exchange processes and on calculations of differential scattering cross sections, it is not possible to determine the elemental sensitivity factor η_i with sufficient accuracy and use it for quantitative analysis using the LEIS method.

[1] Atomic unit of length (au) is the radius of the circular orbital of hydrogen in the Bohr model ($\sim$ 0.0529 nm).

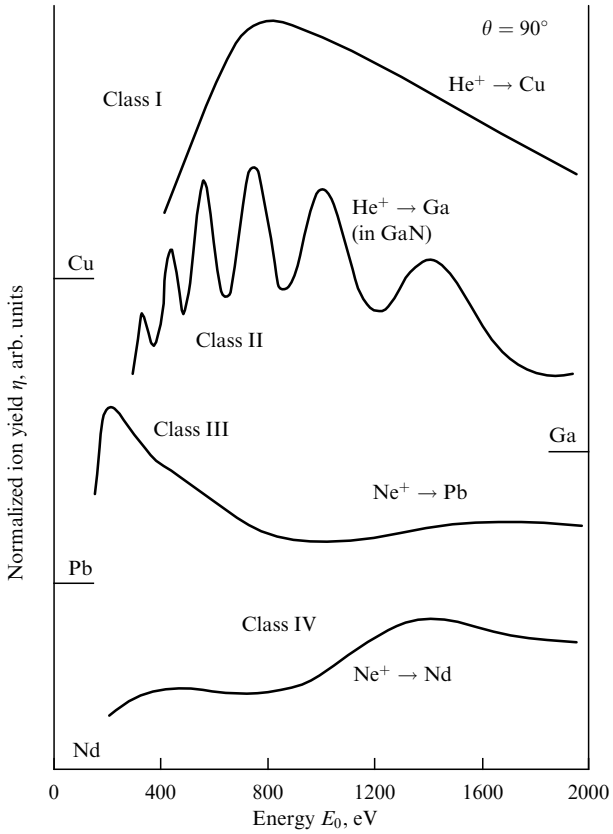

Figure 5. Main classes of experimental dependences of ion yield on primary ion energy obtained in scattering of He^+ and Ne^+ ions from various targets [96].

We now consider the dependence of the ion yield on the primary ion energy for various primary ion/surface atom combinations. This dependence is of importance for testing theoretical concepts of neutralization processes in ion scattering. It is also of practical significance in surface diagnostics using the LEIS method, as it allows one to select an energy range that provides enhanced elemental sensitivity and avoid the influence of matrix effects on the intensity of the scattered ion peak.

One of the first publications on surface diagnostics using the LEIS method [21] presented an experimental dependence $\eta(E_0)$ for He^+ ions scattered from a Cu surface, with a peak at energy $E_0 < 1$ keV and a subsequent smooth decrease in the ion yield intensity. Based on Eqn (9), it can be concluded that the nature of this dependence reflects the change in the product of the scattering cross section $\sigma(\theta)$, which monotonically decreases with increasing primary ion energy, and the ion-survival probability P^+, which monotonically increases upon increasing this energy. Later, in [95, 96], this form of the $\eta(E_0)$ dependence was called classical or conventional. In the same study, it was proposed to divide the $\eta(E_0)$ dependences obtained from the scattering of He^+, Ne^+, and Ar^+ ions from various targets into 4 main classes (Fig. 5 [96]).

Table 1 [96] provides a classification of chemical elements by the form of their $\eta(E_0)$ dependences for three types of primary ions of inert gases (He^+, Ne^+, Ar^+). Of greatest interest is class II, for which oscillating $\eta(E_0)$ dependences are observed. The nature of these oscillations was explained by (quasi)resonant electron exchange with deep levels of surface

Table 1. Preliminary classification of experimental dependences of ion yield on energy of primary ions at scattering angle $\theta = 90°$ [96].

Classes	He^+	Ne^+	Ar^+
I	Al, Si, Ni, Cu, Zn, Zr, Nb, Pd, Ag, Cd, Ta, Au	Zn, Sb, Te, W	
II	Ga, Ge, As, In, Sn, Sb, Tl, Pb, Bi	Ga	
III		Si, S, Ni, Cu, Ge, Pd, Ag, In, Sn, Hf, Pt, Au, Pb	In, Tl, Pb
IV	S, Sc, Te, La, Hf, Ce, Nd, Sm, Gd, Dy, Er, Yb	Cd, La, Ce, Nd, Sm, Gd, Dy, Er, Yb, Tl	Cu, Ge, Pd, Ag, Cd, Sn, Sb, Te, La, Ce, Nd, Sm, Gd, Dy, Er, Yb, Hf, Pt, Au

atoms located within ±10 eV from the first ionization potential of the primary ion. Moreover, this condition must also be supported by the orbital symmetries of the atoms [2]. It was also found that the shape and energy positions of the maxima and minima of the $\eta(E_0)$ oscillations depend on the primary ion/surface atom combinations and the chemical state of the targets. This, as mentioned in Section 1, gave hope that the LEIS method can be applied not only for elemental but also for chemical analysis. Although the ion yield oscillations were measured by varying the primary ion energy, it is more correct to consider this dependence a function of the primary ion velocity rather than the energy. Moreover, the oscillation structure depended on the scattering angle θ, which is characteristic of (quasi)resonant charge exchange processes.

Class III is characterized by a maximum in the $\eta(E_0)$ dependence at energies below 1 keV, along with a broad flat maximum at higher E_0 values, while, for elements assigned to class IV, a smooth increase in the ion yield was observed with increasing primary ion energy. Importantly, no ion yield oscillations were detected for these classes. Later, in review [2], it was proposed to combine classes III and IV based on the fact that existing neutralization and charge exchange models are unable to explain the shape of the $\eta(E_0)$ dependences for the chemical elements included in these classes.

It is worth noting that the authors of [96] called their table preliminary and indicated a specific scattering angle $\theta = 90°$. The table was published in the proceedings of the first conference on inelastic ion-surface collisions (IISC I), which was held in 1976 at Bell Labs (Murray Hill, NJ, USA) [97]. The authors of the review carefully studied the majority of early publications devoted to experimental measurements of the $\eta(E_0)$ dependences [41, 95, 96, 98–105], the US patent on a spectrometer for $\eta(E_0)$ measurements [106], and the latest studies [107, 108] carried out in the HS-LEIS mode. Only article [103] and the patent [106] present experimental dependences obtained during bombardment of targets with primary Ne^+ and Ar^+ ions: in [103], for neon isotopic ions scattered from the surface of solid and liquid gallium, and in [106], for Ne^+/In and Ne^+/Pb combinations and Ar^+/In. All the other aforementioned publications are devoted to $\eta(E_0)$ measurements for He^+ ions scattered from the surface of various targets containing chemical elements of classes I and II. This indicates that the data presented in Table 1 [96] and then refined in review [2] are still preliminary in nature and require additional experimental verification, primarily for the

heavy primary ions Ne^+ and Ar^+. Such verification for Ne^+ ions scattered from Ga and In targets and for atoms of these elements included in the composition of $A^{III}B^{V}$ semiconductor compounds (GaP, GaAs, InP, and InAs) was partially carried out by one of the authors of this review [109, 110] in the energy-mass analysis mode of scattered ions.

Among the latest achievements in calculating the charge function of scattered ions, the wave packet propagation (WPP) method can be noted. This technique, which does not involve the adiabatic approximation, is based on consideration of the tunneling of an active electron from an atomic particle to a metal surface through the potential barrier separating them [6].

The time evolution of the active electron wave function $\Psi(\mathbf{r}, t)$ is calculated by numerically solving the nonstationary Schrödinger equation represented in atomic units:

$$\mathrm{i}\,\frac{\partial\Psi(\mathbf{r},t)}{\partial t} = \left[-\frac{\Delta}{2} + V_{\mathrm{atom}}(r) + V_{\mathrm{surface}}(r)\right]\Psi(r,t)\,. \quad (13)$$

The ground state of the active level of the atomic particle $\Psi_0(r)$ is typically taken as the initial value. The potential relief seen by the active electron during the interaction of the atomic particle with the metal surface is obtained by a simple superposition of the pseudopotentials of the metal V_{surface} and the atomic particle V_{atom}, which is acceptable if the distance between the atomic particle and the surface exceeds 3 au.

Projecting $\Psi(r, t)$ onto the ground state of the electron in the atomic particle yields

$$P(t) = \left|\left\langle\Psi_0(r)\middle|\Psi(r,t)\right\rangle\right|^2, \quad (14)$$

where $P(t)$ is the probability of finding the electron in the ground state of the particle.

Gainullin [6] implemented a 3D version of the WPP method, using three-dimensional potentials that describe the metal surface at the atomic level.

In concluding this section, we note that knowledge of the charge fraction yield of scattered particles significantly enhances the accuracy of the LEIS method for quantitatively determining element concentrations in the surface layer. However, in practice, the calibration sample method, discussed in Section 4, is primarily used for applied problems.

2.3 Advantages of using inert gas ions

We note that inert gas ions do not form strong bonds with the atoms of the surface being studied and therefore, unlike alkali metal ions and active gases, minimally distort its initial state. Furthermore, the high ionization potential of inert gas atoms ensures complete or nearly complete neutralization of ions scattered from layers deeper than the visible surface layer. This implies that the contribution to the surface peak of scattered ions comes primarily from atoms in this layer.

In some cases, alkali metal ions are used for surface diagnostics (see, for example, [12, 13, 113–115] and references therein). When these ions are scattered from a metal surface, a charged fraction yield exceeding 50% is observed. A disadvantage of using alkali metal ions is the significant background due to scattering from atoms located deep in the target and the sensitivity of the ion fraction to the presence of surface contaminants. Scattering of active gas ions was also examined [14–16, 116, 117]. They are primarily theoretical studies aimed at elucidating the mechanisms of negative ion formation during charge exchange. The experiments were conducted at grazing incidence angles and small scattering angles, which increased the time of interaction of the bombarding particles with the surface atoms.

2.4 Effect of multiple scattering and collision inelasticity on scattered ion spectra

Multiple scattering resulting from a series of successive pairwise elastic collisions of the primary ion with target atoms can contribute to the high-energy portion of the scattering peaks shown in Fig. 1a or even form individual peaks with energies higher than that of the scattering peak.

Figure 6 [118] shows the scattering spectrum of Ne^+ ions with an energy of 600 eV at an angle of $\theta = 68^\circ$ from the surface of single-crystal Ni (110). The incidence angle of the primary ions was $\beta = 60^\circ$, and the scattered ions were detected in the forward direction at an angle of 8° to the target surface along the [110] direction. Two scattering peaks are visible in the spectrum: the SS peak of binary single elastic scattering and the DS peak of sequential elastic scattering of neon ions at small angles from two nickel atoms, while the total scattering angle remained equal to 68°. The DS peak can be erroneously interpreted as a scattering peak from heavier atoms that could be present on the Ni target surface, for example, from Pd or Ag atoms. In this case, double scattering is an undesirable effect, but, at the same time, it has been successfully used for surface diagnostics, for example, of $Si_{1-x}Ge_x$ solid solutions [119].

Information on multiple scattering processes and models used to interpret such processes can be found, for example, in [2, 4]. Multiple scattering is primarily used for structural analysis of surfaces, studying interfaces in multilayer structures, determining the positions of adsorbed atoms, monitoring crystal orientation, etc. These issues are discussed in detail in Section 4.

The experimental value of the energy corresponding to the scattering peak may be lower than the energy E_1 calculated using Eqn (1). This shift can be due to instrumental factors, namely, inaccurate determination of the primary ion energy E_0, the scattering angle θ, and the energy analyzer coefficient

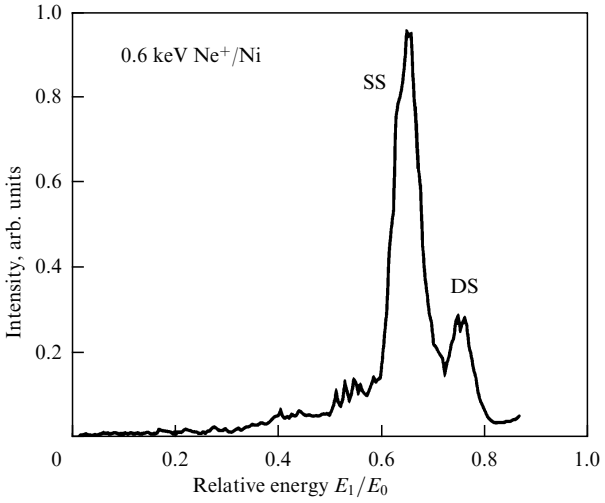

Figure 6. Energy spectrum of 0.6-keV Ne^+ ions scattered at angle $\theta = 68^\circ$ from surface of single-crystal Ni (110) at incidence angle $\beta = 60^\circ$: SS (single scattering) is peak of single elastic scattering, DS (double scattering) is peak of sequential elastic scattering from two atoms [118].

k_{an}. Discrete inelastic energy losses Q (see Eqns (3) and (4)) that occur when the primary ion approaches the target surface, collides with the target atom(s), and then departs from the surface can also lead to a shift in the scattering peak. The nature of these energy losses can be either local, due to the interaction of the electron shells of colliding particles, or continuous (nonlocal), due to the interaction of ions (atoms) with the electron gas of the solid along the entire trajectory of motion.

Many studies examined the physical processes responsible for inelastic energy losses of scattered ions (see, for example, [121–126] and the references cited therein). In the low-energy range of primary ions, the relative magnitude of inelastic energy losses Q/E_0 for most known primary ion/target atom combinations does not exceed 5%. For example, in [125], for the scattering of Ne^+ ions with energies of 500–1950 eV from the surface of a silicon target, the value $Q = 45 \pm 4$ eV was obtained. Similar values of Q equal to 45 ± 5 eV for Ne^+/Al and 55 ± 5 eV for Ne^+/Si were obtained in [123] in the energy-mass analysis mode for the primary ion energy $E_0 > 1.5$ keV, and it was found that, in this energy range, the absolute values of inelastic losses do not depend on E_0. In [89], for Ar^+ ions in the energy range of 3–9 keV scattered from a Ti surface, the value of $Q \sim 90$ eV was obtained. Also in the aforementioned studies, the values of Q were measured for doubly charged Ne^{2+} ions formed during the scattering of singly charged Ne^+ ions from silicon and aluminum targets. For Ne^+/Si, the values obtained were 86 ± 5 eV [125], 110 ± 10 eV [123], and 120 ± 15 eV [89], while for Ne^{2+}/Al, the value of Q was found to be 100 ± 10 eV [123]. It is worth noting that all of the above inelastic energy losses were observed during scattering of primary ions on target atoms with a mass M slightly exceeding the mass of the primary ions M_0, i.e., with large elastic energy losses of the primary ion (see the diagram shown in Fig. 3). In the collision event in this case, the colliding particles come together at a close distance, less than 0.1 nm [125], which facilitates the formation of doubly charged scattered Ne^{2+} ions accompanied by large inelastic energy losses due to the additional ionization of Ne^+ ions. Also, large values of inelastic energy losses were discovered in [124] during scattering of Ar^+ ions with an energy of 5 keV at small angles $\theta = 4-20°$ from the surface of targets, where the mass of the atoms was less than the argon ion mass, i.e., at $\alpha < 1$. For example, for Ar^+/Al at $\theta = 20°$, the value of Q was 160 eV, while for Ar^+/Si at $\theta = 24°$, a value of 135 eV was obtained [124].

In [124], it was shown that, when an aluminum target was bombarded with Ar^+ ions with an energy of 5 keV at a scattering angle of $\theta = 14°$, the energy positions of the maxima of all peaks were shifted toward lower energies due to inelastic energy losses. It should be noted that, despite the rather important results obtained in [124], small-angle scattering of heavy argon ions on light targets is of limited practical interest for applied studies using the LEIS method.

2.5 Evaluation of elemental sensitivity and surface destruction by primary ions

We present data on the detection limits that can be achieved using the LEIS method. Given that the primary advantage of LEIS is its sensitivity to the uppermost visible surface layer, detection limits typically amount to a few percent of the monolayer coating concentration, i.e., $\sim 10^{12}$ atom cm^{-2} for light elements ($M < 20$ amu) using helium as primary ions and $\sim 10^{11}$ atom cm^{-2} for heavy elements using Ne^+ and Ar^+.

Table 2. Estimation of Ni and W target surface destruction during bombardment with 5-keV He^+ and Ne^+ ions.

System	$d\sigma/d\Omega$, Å^2 sr^{-1}	N_s, at/Å^2	Dose, ion/cm^2	Y, at/ion	Fraction of sputtered atoms
He^+/Ni	0.026	0.203	9.022×10^{10}	0.13	5.8×10^{-6}
He^+/W	0.057	0.159	5.254×10^{10}	0.04	1.3×10^{-6}
Ne^+/Ni	0.109	0.203	2.152×10^{10}	1.63	1.7×10^{-5}
Ne^+/W	0.173	0.159	1.731×10^{10}	0.78	8.5×10^{-6}

As an example to evaluate the surface damage by primary ions, we consider the bombardment of Ni and W target surfaces with He^+ and Ne^+ beams with an energy of $E_0 = 5$ keV with the following parameters: irradiated (analyzed) area of 3×10^{-2} cm^2, ring–axis energy analyzer acceptance $\Delta\Omega = 0.07$ sr, and mirror experimental geometry at a 20° incidence angle and 20° emission angle relative to the surface.

The calculated sputtering yields Y and the relative fraction of sputtered atoms at a surface atom density N_s are presented in Table 2 for the cross section of scattering at an angle of 40°, a charged fraction yield of 10%, and a bombarding ion dose required to obtain statistics for 10^5 particles registered by the detector.

As can be seen from Table 2, when using a high-aperture analyzer, the proportion of sputtered atoms is relatively small, although when analyzing multi-component materials with a content of the analyzed element of several percent, this proportion will increase accordingly.

It should be noted that, to reduce the degree of destruction of the analyzed surface in the LEIS method, parameters such as analysis time, beam current, bombardment area size, primary energy, and ion type must be selected appropriately. For He^+ ions and polymer surfaces, the high sputtering yield limits the ion dose to 10^{13} ions cm^{-2}, while for metal surfaces, this dose can be 100 times higher.

2.6 Features of surface diagnostics using LEIS

Surface diagnostics using low-energy backscattered ions, when applied solely to elemental analysis, are reduced to determining the mass and concentration of M_i atoms in the uppermost visible layer of the surface. As mentioned above, the LEIS method is uniquely sensitive to the elemental composition of this layer, allowing for quantitative assessment of concentration. To enhance the reliability of the analysis, it is advisable to have preliminary information on the composition of the target being studied, which helps to optimally select the primary ions, their energy, and current.

A brief digression regarding the concept of 'surface' is appropriate here. If we consider the surface to be the interface between a solid (or other aggregate state of the target being studied) and a vacuum (or another medium, such as a liquid), it refers to a layer several atomic diameters thick, whose properties may differ from those of the bulk target material. Assuming that the diameter of neutral atoms does not exceed 0.5 nm, this value can, as a first approximation, be considered the thickness of an ideal visible surface layer, as shown in Fig. 2. Of course, a real surface, especially in polycrystalline samples, features irregularities and roughness. Their height, which depends on the technology used to obtain and process these samples, can significantly exceed the atomic diameter.

One of the key characteristics of surface diagnostic methods is their surface sensitivity, or information depth, determined by the thickness of the layer from which averaged information on the surface properties, primarily its elemental and chemical composition, is obtained. According to optimistic estimates presented, for example, in [55], the information depth of LEIS does not exceed 1 nm, due to which this method is the most superficial, in the literal meaning of the word, of all surface diagnostic methods. It should be noted that the information depth, even for a target with a perfectly smooth surface, depends on its properties, such as work function and conductivity, on the energy, mass, and ionization potential of the primary ions, the angles of incidence and scattering, and other physical and instrumental factors.

Already in the first publications on the application of LEIS, for example, the analysis of polar faces of CdS and ZnS crystals [21–23] showed that the high ionization potential of inert gas atoms ensures complete or almost complete neutralization of ions scattered from layers deeper than the visible surface layer, i.e., the contribution to the surface peak of scattered ions comes mainly from atoms from this layer. Later, Bauer et al. [126], using a more sophisticated experimental technique of time-of-flight (TOF) analysis of all scattered particles (neutral and positively charged) with additional modeling using the MARLOWE program, confirmed that the main contribution to the surface peak comes from the two upper layers of the surface of the sample under study. It should be noted that the time-of-flight technique for analyzing the backscattered spectrum of atoms [127] allows enhanced accuracy of quantitative analysis and is successfully applied up to energies of 100–200 eV, i.e., in the hyperthermal energy range discussed in Section 5 of our review.

The scattering angle θ in most LEIS setups is selected in the range of 90°–145° to ensure separation of scattering peaks and reduce the undesirable contribution to the energy spectra from multiple scattered ions, while maintaining a sufficiently high sensitivity, which decreases with increasing scattering angle due to a decrease in the scattering cross section $\sigma(\theta)$. The scattering angle θ is determined by the relative positions of the primary ion source and the energy analyzer in the vacuum chamber, and this angle usually cannot be changed. Varying it requires a device for rotating the ion source or scattering plane analyzer, which complicates the design of the vacuum chamber and is rarely implemented in practice. In contrast, the incident angle of the primary beam β can be varied over a wide range by rotating the sample using a manipulator. Preferably, either normal incidence, when $\beta = 90°$, or specular scattering geometry, in which $\beta = \theta/2$, is used. In setups designed for surface structure studies using the LEIS method, the scattering/emission and incidence angles are selected to be less than 90°.

$^4He^+$ ions are most often used as primary ions in the LEIS method, as are sometimes isotopic $^3He^+$ ions. For helium ions, sputtering of the original surface during analysis is minimal, and the relative mass $\alpha = M/M_0 > 1$ for all chemical elements except hydrogen. As already mentioned, the mass resolution $\Delta M = 2$ amu can be achieved for primary $^4He^+$ ions in the range of surface atom masses of 5–26 amu; for $^{20}Ne^+$, in the range of 21–55 amu, and for $^{40}Ar^+$, in the range of 41–78 amu.

Note that, when calculating the mass spectral resolution of the LEIS method using Eqn (7), it was assumed that the shape of the scattering peaks is described by the normal distribution law without the contribution of re-ionized and multiply scattered ions and sputtered secondary ions. Under real experimental conditions, the value of the mass spectral resolution may be worse than that calculated using Eqn (7); nevertheless, study [44] showed that the scattering peaks of Ne^+ ions can be separated from those of elements with similar masses, Ni and Cu, and the surface segregation of elements in the alloy can be studied.

However, problems with the mass spectral resolution of the LEIS method exist, and mathematical processing of the experimental data can help resolve them. An example is the processing of the scattering spectrum of primary Ne^+ ions with an energy of 5 keV from the surface of a multicomponent alloy consisting of Cr ($M \cong 52$ amu), Mn ($M \cong 55$ amu), Fe ($M \cong 56$ amu), Ni ($M \cong 59$ amu), and Co ($M \cong 59$ amu). The measurements were carried out in HS-LEIS mode [56]. Only three scattering peaks could be distinguished in the experimental spectrum, which corresponds to the mass spectral resolution for Ne^+ ions calculated using Eqn (7). The authors of [56], knowing the composition of the sample in advance and calculating the energy positions of the scattering peaks for its components, processed the experimental spectrum using the deconvolution method, similar to the way this is done when processing XPS spectra. The scattering peak shape was assumed to be Gaussian, and the contribution from sputtered secondary ions was subtracted from the experimental spectrum. After mathematical processing, five scattering peaks were identified in the spectrum, corresponding to the number of chemical elements contained in the alloy under study.

Continuing to discuss the measurements of scattering peak intensity, we note that either the scattering peak amplitude (maximum value) or the average value calculated during discrete energy scanning of the analyzer for the intensity maximum and several values before and after the maximum can be used as its value. This improves the signal-to-noise ratio and increases the accuracy of measurements, especially in quantitative analysis using the LEIS method. When studying neutralization processes, for example, when determining the characteristic velocity v_c in Eqn (12) [90], the scattering peak intensity can be integrated at the half-maximum (FWHM) level.

The primary ion energy E_0 is typically selected in the range of 1–3 keV and sometimes up to 5 keV. For example, on a Qtac^{100} spectrometer, most measurements using primary helium ions are carried out at $E_0 = 3$ keV [56]. Knowing the $\eta(E_0)$ dependence, one can select an E_0 value that provides enhanced sensitivity. However, it should be taken into account that, with increasing primary ion energy, also increased is the undesirable contribution to the scattering spectra from re-ionized scattered ions (see Fig. 1) and, when using Ne^+ and Ar^+ primary ions, also from sputtered secondary ions.

The primary ion current I_0 is typically selected in the range not exceeding a few μA. To increase elemental sensitivity, according to Eqn (8), I_0 must be increased, but this enhances the destruction/alteration of the initial surface state due to ion sputtering, implantation, and the formation of radiation effects, especially when using primary neon and argon ions. Nevertheless, in many experiments, the surface of the studied samples is pre-cleaned by bombardment with heavy ions with an energy of 5 keV [56].

An ideal LEIS experiment assumes that no more than one primary ion hits each surface atom during the analysis period. Assuming an atomic concentration on the surface of $N \sim 10^{14}$ atom cm^{-2} and a primary ion current density of

$j_0 \leqslant 100$ nA cm^{-2}, the time of 'nondestructive' surface analysis, during which the required energy range E_1 can be scanned, should not exceed 100 s. In this case, it is necessary to ensure a high vacuum (10^{-6}–10^{-7} Pa) near the surface of the sample being studied to avoid contamination of the original surface with adsorbed atoms of residual gases.

2.7 Computer simulation of ion-surface interaction

Before proceeding to a brief overview of computer programs developed for modeling ion-surface interaction processes, we provide a link to a convenient calculator (LEIS Energy Calculator [128]), which allows computing the energy of scattered ions using Eqn (1) and estimating other scattering parameters for the Ziegler–Biersack–Littmark [72] and Thomas–Fermi–Molière [76] interaction potentials.

The authors of [129] proposed using the binary elastic collision approximation for computer simulation, in which the scattering of atomic particles in a solid is considered a sequence of binary collisions of the incident particle with atoms of the solid. In this case, the particle trajectory is replaced by the asymptotes of the trajectory. An important step in the development of computer modeling was the work of Ziegler, Biersack, and Littmark on the analysis of ion ranges in solids, which led to the creation of the widely used SRIM (Stopping and Range of Ions in Matter) code [130].

Table 3 presents some computer programs based on the binary collision approximation.

At collision energies below 50 eV, the applicability of the binary collision approximation is violated. At low energies and with grazing incidence of the beam on the target, it is necessary to take into account the interaction of the incident particle with a large number of atoms. Examples of the application of trajectory calculation methods in this case can be found in [6, 138].

At low energies, the molecular dynamics (MD) method is widely applied. This method calculates the motion of all interacting atoms as a function of time. The trajectories of atoms and molecules are determined by numerically solving Newton's equations of motion, where the forces between particles are often calculated using interatomic many-particle potentials. Calculations using this model require significant computing power.

Table 3. Computer codes based on binary collision approximation.

Program	Authors	Features	References
ACAT	Takeshi, Yamamura	Initially amorphous targets	[131]
MARLOWE	Robinson, Torrens	Initially crystalline targets	[132, 133]
SDTrimSP	Biersack, Eckstein	Static and dynamic calculations. Sequential and parallel calculations	[134]
SRIM	Biersack, Ziegler	Amorphous targets	[130]
OKSANA	Shulga	Crystal, polycrystals, and amorphous targets	[135]
SARIC	Bykov et al.	Crystals	[136]
Ioffe Institute	Meluzova et al.	Crystal, polycrystals, and amorphous targets	[137]

For MD calculations, the LAMMPS code [139] (Large-scale Atomic/Molecular Massively Parallel Simulator) is often used. Developed at Sandia National Laboratory (Livermore, USA), the LAMMPS program allows modeling interactions with targets in liquid, gaseous, and solid states. The code incorporates various types of interatomic interaction potentials. Also noteworthy are the KALYPSO computer program [140], developed by M.A. Karolewski for MD calculations of collisions in metal targets, and the SAFARI program [141], which allows the molecular-dynamics simulation of ion scattering spectra in the low- and hyperthermal-energy range (1–1000 eV).

3. LEIS instrumentation

Figure 7 shows a simplified block diagram of an LEIS spectrometer. The main components are the primary ion source and the analyzer. Typically, sources employing ionization of the working inert gas by an electron beam generated by a heated cathode are used. A mass separator that allows the ion beam to be purified from impurity ions is either a straight-through mass filter with crossed electric and magnetic fields (Wien filter) (see, for example, [142]) or a sector magnetic analyzer. The neutral particles, which can reduce the dynamic range of depth profiling analysis during surface sputtering by an ion beam, are eliminated by deflecting the ion beam axis by several degrees from the axial position due to mechanical displacement. When using a sector magnetic analyzer, neutral particles are removed from the beam concurrently with impurity ions. A pulse modulator is required for operation with a time-of-flight analyzer. Focusing and scanning of the ion beam is provided by one or more electrostatic lenses and an electrostatic XY deflector. All of the listed devices are commonly referred to as 'ion guns' or 'primary ion beam columns,' while power supplies and the device for injecting inert gas are omitted in Fig. 7. The vacuum in the analytical chamber ($10^{-6}-10^{-7}$ Pa) is provided by turbomolecular pumps, or less commonly by sorption magnetic discharge or cryopumps. The ion gun can be equipped with turbomolecular pumps for differential pumping of the inert gas; in the simplest version, purified gas flows in up to a pressure of 10^{-3} Pa (without pumping) directly into the analytical chamber housing the ion gun.

The primary ion beam energy E_0 is selected in the range of 0.5–5 keV with a sample current I_0 ranging from fractions of a nA to several μA. The main requirement for the ion beam is a

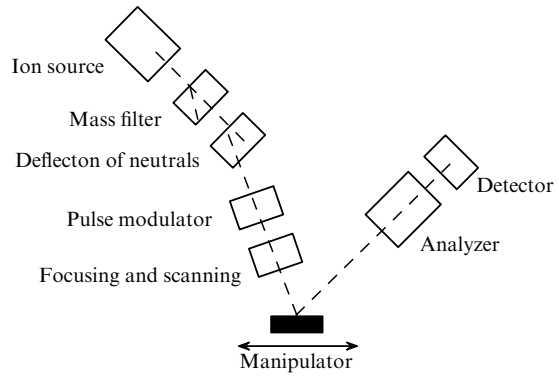

Figure 7. Simplified block diagram of LEIS spectrometer [2]. Figure does not show power supply units, inert gas inlet device, vacuum pumps and vacuum control equipment, or system recording scattered ion signal.

small energy spread, less than $5 \times 10^{-3} E_0$, which is necessary to reduce ΔE_1, and a small angular spread (1–2°), i.e., parallel ion trajectories in the beam to reduce $\Delta\theta$. For this reason, strongly focused ion beams are typically not used in LEIS, and measurements are carried out with ion beam diameters (spatial resolution) of 10–100 μm [55]. These requirements are met in many commercial ion guns, such as the IQE12/38 (SPECS, Germany [143]), which can be additionally equipped with a Wien filter and operate in differential pumping mode.

The manipulator provides sample movement in three directions XYZ and rotation in one or two planes without disrupting the vacuum in the analytical chamber. Manipulators can also be equipped with heating and cooling devices, along with automatic sample movement and position control systems.

Various types of electrostatic analyzers are used as energy analyzers [144]. In the first LEIS setups (e.g., [21]), this was a 127° cylindrical sector deflector, followed by sector and 180° spherical deflectors and cylindrical mirror analyzers (CMAs). Setups equipped with such energy analyzers with electron, ion, and X-ray beam sources are usually combined spectrometers, as for example, ESCALAB (Thermo Fisher Scientific, UK [145]), in which the main diagnostic methods are photoelectron and Auger electron spectroscopy. In such spectrometers, to detect the signal of scattered positive ions, it is necessary to reverse the polarity of the voltages on the electrodes of the input optics and the deflection plates of the analyzer and on the detector. Another approach is the construction of laboratory (homebuilt) setups using commercially available analyzers, ion guns, vacuum equipment, and other necessary components and units (e.g., [146]). Due to problems related to acquiring analytical equipment for surface diagnostics in the USSR, most ion scattering spectrometers of that time were laboratory setups designed and made by researchers themselves. Descriptions of such setups can be found in monographs [4, 36, 43].

Of particular interest is the complex experimental setup [147], developed and produced at NITI using the component design of electron and ion spectrometers [148]. A distinctive feature of this setup was a 180° spherical deflector mounted on a rotating platform, which allowed the scattering angle θ to be varied from 0 to 160° with an accuracy of 1°. The energy resolution of this analyzer was $(\Delta E/E)_a = 0.3\%$ with an angular resolution of $\theta = 1.5°$. The ability to directly inject the primary beam into the analyzer allowed highly accurate measurement of the ion beam parameters (E_0 and ΔE_0), estimation of its diameter, and determination of the analyzer coefficient, which enhanced the reliability of interpreting the energy spectra of scattered ions and ionized recoil atoms.

Recall that, to achieve high sensitivity, LEIS requires a strictly defined scattering angle θ with a minimal $\Delta\theta$ value of $\sim 1° - 2°$ at the largest possible azimuthal entrance angle to the analyzer. A large azimuthal entrance angle is virtually not possible to achieve for the aforementioned analyzers due to the limited dimensions of their input apertures (slits) at fixed θ and $\Delta\theta$.

When using a standard CMA in LEIS mode with an axial electron gun inside the analyzer and ion guns located outside the analyzer, such as employed in the UAE.OPR-5-007, a combined spectrometer developed at NITI, a mechanical shutter was used to fix the scattering angle. This shutter was positioned in front of the analyzer entrance and moved by a special manipulator.

To increase the azimuthal entrance angle of the CMA in LEIS mode, it was proposed to use an axial primary ion source [149–151]. In this approach, the primary ions were directed normal to the sample surface, and backscattered ions were collected at a fixed scattering angle ($\theta \geqslant 135°$) and an azimuthal entrance angle of 360°. The detector used was either a standard secondary electron multiplier (SEM) located inside the CMA [149, 150] or a more complex ring SEM, which allowed the primary ion source to be located outside the analyzer. A setup with such an analyzer and ion source, which was developed by Brongersma's group, was named Nodus [151].

In [150], it was proposed that a hybrid source of charged particles with a cold cathode be placed inside the CMA, which could generate both ion and electron beams for surface analysis using LEIS and Auger electron spectroscopy. However, this approach was not developed further due to the insufficient performance of the hybrid source in both operating modes.

The idea of using an ring SEM with an external axial ion gun was further developed and refined by Brongersma's group. The CMA was replaced with a dual toroidal electrostatic analyzer [152], which made it possible to simultaneously analyze scattered ions by energy and azimuthal angles, i.e., obtain information not only on the elemental composition of the surface, but also on its structural features. The experimental setup with a toroidal analyzer was named EARISS (Energy and Angular Resolved Ion Scattering Spectrometer) [153].

This setup was subsequently improved [154], and, on its basis, IONTOF, in collaboration with Brongersma's group, developed the commercial Qtac^{100} spectrometer, which used a dual toroidal analyzer. Figure 8a, b shows a schematic representation of such an analyzer with an axial ion source, a position-sensitive detector, and a pulse modulator, while Fig. 8c presents its external appearance [54, 55]. The toroidal analyzer allows scattered ions to be analyzed over a wide energy range (5–10% of the analyzer's transmit energy) without loss of energy resolution $(\Delta E/E)_a$, even though the trajectories of these ions within the analyzer differ from one another. A position-sensitive detector registers ions with various trajectories, providing information on the surface structure. A pulse modulator of the primary ion beam is necessary for implementing time-of-flight filtering (separation) of scattered and sputtered secondary ions, which contributes to an increase in the signal-to-noise ratio and enhances the sensitivity of the analysis.

It should be noted that, already in the early 1980s, 3M (USA), using the first LEIS systems with a sector cylindrical energy analyzer [21], began the manufacture of specialized ion scattering spectrometers capable of measuring the dependence of ion yield on the energy of primary ions. However, this production, which was small scale, was not further developed. In the 1980s, NITI produced several UAE.OPR-5-007 combined spectrometers, which were successfully used at enterprises of the USSR Ministry of Electronic Industry.

We now return to the block diagram of the LEIS spectrometer (see Fig. 7). An electrostatic analyzer is not the only instrument that can be used for the energy analysis of backscattered ions and ionized recoil atoms. Time-of-flight analyzers have also been used for these purposes since the late 1980s. Such analyzers made it possible to detect hydrogen along with the neutral component of scattered ions and recoil

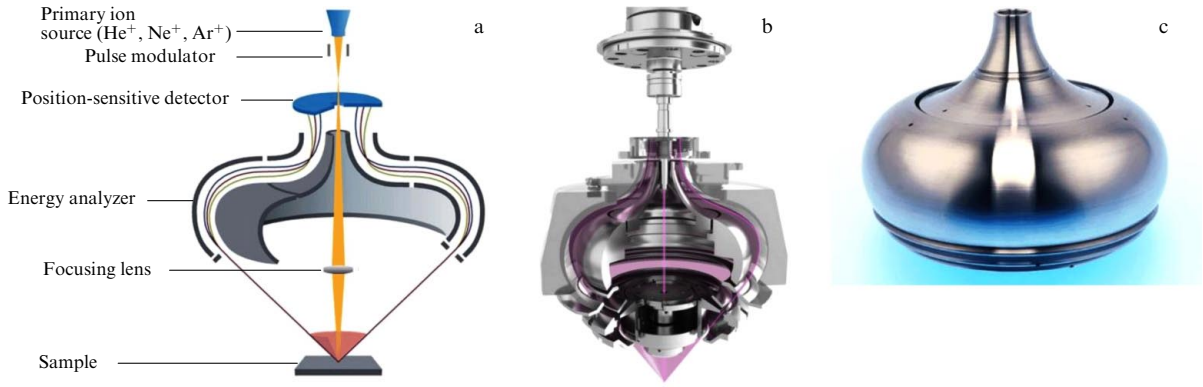

Figure 8. Schematic representation of dual toroidal analyzer with axial ion source, position-sensitive detector, and pulse modulator (a); sectional view (b), and external view of this analyzer (c) [54, 55].

atoms. TOF analyzers were primarily used in laboratory setups for surface structural analysis [57] and for studying neutralization processes [126]. Descriptions of such setups can be found, for example, in [57, 127, 155, 156]; they also operate effectively in the range of medium energies of scattered ions (the MEIS method) [157, 158]. Note that pulse modulation of the primary ion beam is required for operation with a time-of-flight analyzer (see Fig. 7).

4. Application of LEIS method for solving applied and basic problems

The application areas of LEIS are quite diverse, but they are all united by the method's ability to provide unique surface sensitivity combined with the ability to quantitatively evaluate measurement results. One can distinguish the investigation of the surfaces of catalysts, glasses and various minerals, metal alloys, thermionic emitters, etc. Some of these studies have already been cited in this review, for example, article [49] devoted to examination of oxide cathode activation processes. A detailed analysis of the main results of LEIS application before the early 2000s can be found in the monographs by Mashkova, Molchanov, and Kurnaev [4, 43] and in the review by Brongersma et al. [2]. The specifics of HS-LEIS application are discussed in a practical guide to the interpretation of backscattered ion spectra [56].

We discuss the specifics of using calibration samples with known concentrations of chemical elements for the quantitative interpretation of LEIS experimental data.

Both pure and multi-component samples, such as metal alloys, are used as calibration samples. It should be noted that the elemental composition of multi-component samples must be pre-measured using another independent quantitative method with a sensitivity at least equal to that of LEIS. Furthermore, the information depth of this method should be approximately the same as that of LEIS. Both of these conditions are quite difficult to fulfill, especially the second requirement, which concerns the depth of the analyzed layer, since the composition of the upper surface layer, which is the subject of LEIS studies, may differ from the bulk composition of the sample due to the presence of surface contaminants, including oxides, segregation of individual components, and selective sputtering during surface cleaning with an ion beam.

For clean samples, the elemental sensitivity η_i can be determined based on Eqn (8) by normalizing the scattering peak intensity I_i to the primary current I_0. The elemental sensitivity often includes an instrumental factor A and a coefficient R, which takes into account the surface roughness of the samples. In the late 1990s, Brongersma organized a round robin LEIS experiment [159], the purpose of which was to compare the elemental sensitivity values obtained for pure polycrystalline samples of Al, Ni, Cu, Pd, and Pt in five laboratories based in the Netherlands, Germany, Italy, France, and Belgium. All the samples listed in Table 1 of [96], except platinum, belong to class I with the conventional character of the $\eta_i(E_0)$ dependence. As for Pt, it is assigned in this table to class III for primary Ne^+ ions, and there are no data for He^+ ions for this chemical element either in Table 1 or in review [2]. All spectrometers used in the round robin experiment were laboratory setups equipped with cylindrical or spherical electrostatic energy analyzers with approximately the same solid entrance angles $\Delta\Omega$. Helium isotopic ions ($^3He^+$ and $^4He^+$) and Ne^+ with energies of 0.6–3.5 keV were used as primary ions, with some ion sources equipped with magnetic mass separators. The sample surfaces were pre-cleaned by bombardment with Ar^+ ions with energies of 2–3 keV. The scattering angles θ were 90°, 135°, 137°, 139°, and 142°, with primary beam incidence angles β ranging from 45° to 90°.

As a result of the experiments, it was found that the spread of elemental sensitivity η_i values for the studied metal samples did not exceed ±20%, and, within each individual laboratory, the data reproducibility was better than 10%. It was not possible to verify the nature of the $\eta_i(E_0)$ dependence for the studied elements, since the elemental sensitivity values were normalized to data for copper samples. Additionally, the surface composition of the $Cu_{55}Pd_{45}$ alloy was quantitatively measured in three laboratories — in Eindhoven, Florence, and Garching-bei-Munich — using a copper calibration sample in a single experiment (*in situ*). The average atomic concentration of Cu in this alloy was 58 ± 3 at.%, while, according to XPS measurements conducted in Garching, it was 54.5 at.%.

A quantitative analysis of the surface composition of CuPd calibration alloys with various component concentrations was carried out using the LEIS method in [160]. Using the RBS method, which can be considered completely quantitative, since it does not require additional calibration, the copper concentration in these alloys was measured; it was found to be equal to 20, 40, 55, 75, and 85 at.%. In addition, the elemental sensitivity for pure Cu and Pd samples was determined under the same experimental conditions. The

measurements of the relative intensity of the scattering peaks Ne^+/Cu and Ne^+/Pd yielded a virtually linear dependence of the intensities $I_{Cu}(I_{Pd})$ for samples with different copper concentrations, which indicates the absence of matrix effects, i.e., the influence of the chemical environment of the atoms of the studied samples on the ion-survival probability, P^+, of the scattered ions. This confirms the feasibility of quantitatively analyzing such alloys using the LEIS method. It was shown that sulfur, a surface contaminant, segregates on the alloy surface at temperatures above 650 °C during thermal cleaning, with sulfur atoms primarily located on copper atoms. It was also found that copper atoms are preferentially sputtered during ion bombardment.

The absence or negligible influence of matrix effects on the intensity of scattering peaks is a significant advantage of the LEIS method. In [161], it was shown that, during the scattering of $^3He^+$ and $^4He^+$ ions with energies of 1–3.5 keV from polycrystalline $Ni_{80}Pt_{20}$ and $Ag_{80}Al_{20}$ alloys and NiO and Al_2O_3 oxides, the chemical composition of the samples under study did not affect the ion-survival probability of the scattered helium ions. However, it was found that the P^+ values for the single-crystal NiAl{110} alloy were significantly lower than those for the polycrystalline sample of pure aluminum. The authors of [161] attributed this observation to the influence of matrix effects, without specifying the mechanism for this influence. In our opinion, the difference in the intensity of the scattering peaks from the surface of the single-crystal alloy and the polycrystalline calibration sample could be influenced by the different structure of their surfaces, primarily the surface roughness of the polycrystalline samples.

In [162], CaF_2 powders and single crystals were quantitatively analyzed in the HS-LEIS mode (3 keV He^+, $\theta = 145°$) using a single-crystal LiF(001) sample and metallic Ca, a thin layer of which was deposited in a vacuum onto the surface of an SiO_2 substrate, for calibration. The F/Ca surface atomic concentration ratio was found to be 2.3 ± 0.1, being the same for both powdered and single-crystal calcium fluoride. The surface roughness of the powders studied affected the intensity of the calcium and fluorine scattering peaks, decreasing it by 0.77 ± 0.03 compared to the single-crystal $CaF_2(111)$ sample.

The influence of matrix effects on the results of quantitative analysis is particularly noticeable in secondary ion mass spectrometry, where the probability of ionization of sputtered particles (secondary ions) depends both on the electronic and vibrational state of these particles and on their chemical environment in the sample under study. Unlike LEIS, SIMS quantitative impurity analysis utilizes relative sensitivity factors (RSFs) [163, 164],

$$\mathrm{RSF}_i = C_i \frac{I_\mathrm{m}}{I_i}\,, \tag{15}$$

where C_i is the bulk concentration of impurity atoms, and I_m and I_i are the intensities of selected isotopic mass peaks of secondary ions of the matrix and impurity, respectively.

RSF values are determined by analyzing calibration samples, typically prepared by ion implantation of the impurity into a known matrix. A linear relationship between the intensities of impurity and matrix mass peaks is only observed for $C_i < 1$ at.%, i.e., when the concentration of implanted impurity atoms has virtually no effect on the matrix composition. RSF values depend on the matrix, the type of mass spectrometer (magnetic or quadrupole), the primary ions, and other experimental characteristics. Unlike LEIS, quantitative analysis of the composition of multi-component samples using SIMS is a challenging task, although satisfactory results have recently been obtained in the depth profiling analysis of binary and ternary semiconductor structures based on silicon, germanium, and tin [165, 166].

Let us also recall that, when deriving Eqn (1), it was assumed that the target atoms remain motionless (frozen) upon collision with the primary ions, since the interaction time of the ion with the target atom ($\sim 10^{-15}$ s) is much shorter than the period of its thermal oscillations ($\sim 10^{-13}$ s). In recent years, many studies have been conducted to numerically simulate the influence of thermal oscillations on the spatial distribution of scattered ions (see, for example, [167, 168]). The results of such studies, which have provided information on the amplitude of thermal oscillations, are of interest in the study of fundamental processes in solids. For practice, it is of importance that LEIS surface analysis can be carried out at temperatures significantly above room temperature, with the energy positions of the scattering peaks corresponding to those calculated using the binary elastic collision model, and the peak shapes changing only slightly over a wide temperature range.

As an example, Fig. 9 [49] shows the spectra of He^+ and Ne^+ ions with energies of $E_0 = 1.5$ keV scattered at an angle of $\theta = 74°$ from the surface of an oxide cathode prepared using the binary carbonate $BaCO_3$ and $SrCO_3$. The spectra displayed in Fig. 9 show the change in the elemental composition of the oxide cathode surface during its degassing, activation, and subsequent cooling to room temperature. Without going into the details of the operation of the oxide thermionic cathode (the necessary information can be found, for example, in [49]), we note that the energy positions of the scattering peaks and their shapes for the activated and then cooled cathode (Figs 9b–d) remained virtually unaltered. In the case of the unactivated cathode (Fig. 9a), the position, shape, and amplitude of the peaks were affected by the charging of the cathode surface, which occurs during ion bombardment of its surface. During activation, the electric charge on the cathode surface was eliminated by the formation of a conductive monolayer of metallic barium doped with strontium.

4.1 Elemental and chemical analysis of surface and subsurface layer composition of various materials and devices

In discussing the practical application of the LEIS method, we sought to avoid repeating results previously published in the various monographs and reviews listed in Section 1. Instead, we focused on the analysis of liquid surfaces, studies of nanoparticles and clusters, cultural heritage objects, microelectronic materials and devices, including their depth profiling analysis, and the feasibility of chemical analysis.

One of the first studies on the analysis of liquid media [169] was devoted to investigating the elemental composition and structure of the double electrochemical layer formed on the surface of an Ag electrode immersed in a solution of common salt. For LEIS measurements, He^+ ions with an energy of 2 keV and a sample current of 30 nA were used. Using layer-by-layer analysis in combination with XPS, we found the formation of a monolayer of Cl^- anions on the

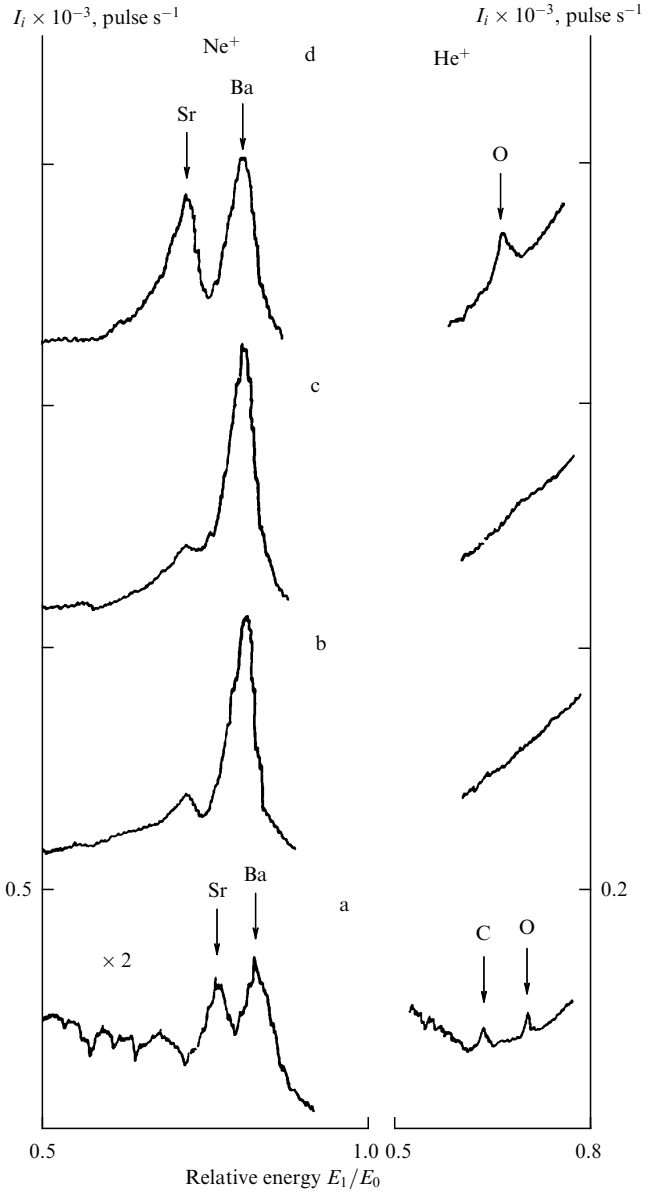

Figure 9. Spectra of He^+ and Ne^+ ions ($E_0 = 1.5$ keV, $\theta = 74°$) scattered from surface of oxide cathode, measured at various temperatures: (a) unactivated cathode at $T = 300$ K, (b) de-gassing at $T = 1100$ K, (c) activation at $T = 1200$ K, (d) cooling to $T = 300$ K [49].

electrode surface, which preceded the formation of the bulk AgCl compound. Experiments were conducted *ex situ* (outside the electrochemical reactor), because it was not possible to provide the high-vacuum conditions required for LEIS and XPS measurements directly *in situ* (within the electrochemical reactor).

Subsequently, room-temperature ionic liquids (RTILs) [170] — liquids with a melting point no higher than 100 °C — have become one of the primary subjects of ion-scattering studies of liquid surfaces. These liquids consist of organic cations and organic or inorganic anions. A distinctive feature of RTILs, referred to in this review simply as ionic liquids (ILs), is that they exhibit virtually no evaporation, due to which they can be studied under high and ultrahigh vacuum conditions.

Currently, more than 10,000 various ILs have been synthesized, many of which are now applied in power generation, biotechnology, 'green chemistry,' analytical instrumentation, and space technologies (see, for example, [171] and references therein). According to modern theoretical and experimental concepts [172], ILs are complex nanostructured liquids consisting of polar and nonpolar regions with ordered formations: domains, ion pairs, quasimolecular packings, and associates. Of interest is the elemental composition and structure of the outer layer of the IL surface. In [173], the LEIS method using He^+ ions was used to show that the surface of the ionic liquid $[C_4mim][Tf_2N]$, the full name of which is 1-butyl-3-methylimidazolium bis(trifluoromethylsulfonyl)imide, mainly contains fluorine, while, according to XPS measurements made in the same study, the surface composition of the IL did not differ from the bulk composition of the IL.

More detailed studies of ILs were conducted in [174]. A total of 23 ionic liquids consisting of various cations and anions were investigated. The studies were carried out using He^+ ions ($E_0 = 3$ keV, $\theta = 145°$) in a vacuum of 10^{-6} Pa. In simple chemical terms, the main result is that the probability of the presence of cations, i.e., positively charged atoms and atomic complexes, on the surface of ILs is very small, while anions were present on the surface of all ILs studied. The existence of the most probable surface orientation of anions was also discovered, which is important for controlling the reactivity of ionic liquids.

The results of ion scattering studies of the surface of various liquid media, including ordinary and ionic liquids, surface-active solvents, foam films, and biological systems, are presented in reviews [175, 176]. In addition to the LEIS method used for the studies, medium- and high-energy ion scattering (MEIS and RBS, respectively) and the neutral impact collision ion scattering spectroscopy (NICISS) method were employed. The authors of reviews [175, 176] note that state-of-the-art ion scattering methods represent a powerful analytical tool, often the only option, for determining the quantitative elemental composition of the outer layer of liquid surfaces and for measuring the distribution profiles of element concentrations and structural (orientational) features in the near-surface region.

In [177], the surface composition of binary silicate glasses containing modifying oxides of sodium, cesium, and barium was examined. The experiments were conducted using He^+ ions ($E_0 = 4$ keV, $\theta = 145°$). A significant difference was found in the elemental composition of the surface of all the studied glasses before and after their fracture in a vacuum. The change in the scattering peak of the modifying element Ba (Fig. 10 [177]) is especially noticeable for Ba_3S glasses with a bulk composition of $3SiO_2 \cdot BaO$. The ratio of the intensities of the scattering peaks of silicon and oxygen remained virtually unchanged. The results obtained allowed drawing conclusions about the processes accompanying the fracture of glasses and, based on this, improving their strength properties.

The analytical capabilities of LEIS are not limited to surface analysis. Researchers and specialists developing new materials and devices are typically interested not only in the composition of the topmost surface layer, but also in the distribution profiles of elements in the near-surface region. Depth profiling analysis with ion beam sputtering is one of the most suitable tools for these purposes (see, for example, [178] and references therein). As early as 1993, a European patent [179] was issued that, in addition to recording the scattering spectra of He^+ ions, proposed sequentially remov-

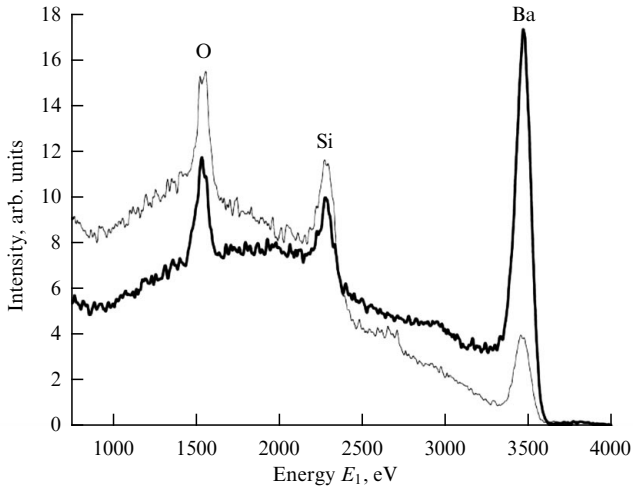

Figure 10. Spectra of He^+ ions ($E_0 = 4$ keV, $\theta = 145°$) scattered from surface of binary silicate glass Ba_3S, measured for initial state (thin line) and after destruction in vacuum (thick line) [177].

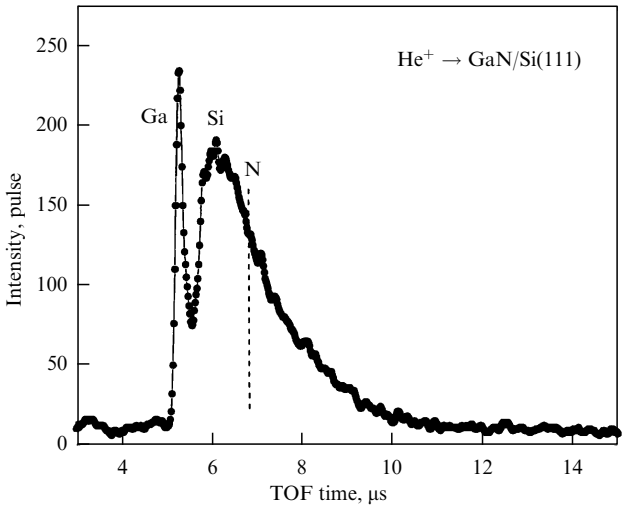

Figure 11. TOF spectrum of He^+ ions ($E_0 = 3$ keV, $\theta = 135°$) scattered from surface of Ga-N film (3.3 monolayers) deposited on Si(111) [187].

ing/sputtering the surface layers of the studied objects with heavier neon or argon ions, i.e., performing depth profiling LEIS analysis.

Currently, the Qtac^{100} system enables depth profiling analysis using two independent ion beams (LEIS Dual Beam Depth Profiling) [180]. An example of depth profiling LEIS analysis using a Qtac^{100} setup with 6 keV He^+ ions for analysis and 5 keV Ne^+ ions for sputtering can be found in study [181], which investigated Y-type zeolites. The studies were conducted using not only LEIS, but also laboratory-scale X-ray photoelectron spectroscopy (with a fixed X-ray beam energy) and synchrotron radiation, i.e., with variable probe radiation energy. The results of measurements by all methods, including depth profiling analysis data from laboratory XPS with argon ion sputtering of samples, showed enrichment of the near-surface layers with aluminum, the most accurate measurements of the surface concentrations of Si and Al being made by the LEIS method.

The composition of a layer formed on the surface of a CdTe single crystal after etching with bromomethanol was investigated in [182] using dynamic LEIS (D-LEIS) with only 5-keV Ne^+ ions for both analysis and layer-by-layer sputtering. This layer was found to be rich in tellurium at the CdT_4 level; the tellurium content decreased exponentially into the sample, and at a depth exceeding 6 nm, the surface layer composition became stoichiometric. These samples were concurrently studied using angle-resolved X-ray photoelectron spectroscopy (ARXPS) [183] in conjunction with D-LEIS. It was shown in [182] that D-LEIS provides more detailed information on the surface layer composition than ARXPS.

Depth profiling LEIS analysis can also be carried out using He^+ ions alone. The sputtering yield in this case is small (~ 0.1 atom/ion [184]), but removal/etching of surface layers still occurs. By analogy with D-LEIS, this method of depth profiling analysis can be called static S-LEIS. In [185], S-LEIS was used to measure the palladium concentration in Pd–Pt bimetallic clusters deposited on a carbon surface by laser evaporation of alloys. The experiments were carried out on an ESCALAB 200R setup (Fisons Instruments, UK) with He^+ ions ($E_0 = 4$ keV, $\theta = 145°$) at a sample current of 10 nA. Pd and Pt concentrations were quantitatively assessed with calibration using single-crystal samples of Pd(100) and Pt(111). Based on the results of S-LEIS measurements for clusters with the bulk composition $Pd_{65}Pt_{35}$, it was found that the cluster surface was rich in palladium. Similar results were obtained for clusters with the bulk composition $Pd_{17}Pt_{83}$, and Monte Carlo simulations confirmed the experimental data.

In [186], gold nanoparticles for biomedical applications were studied. The analysis was carried out using 3-keV He^+ ions, and sputtering was conducted with 500-eV Ar^+ ions. It was shown that self-assembled monolayers (SAMs) of Au nanoparticles functionalized with $C_{16}COOH$ acid were formed at a SAM thickness of about 14 nm.

The time-of-flight version, TOF-LEIS, was used in [187] to study the growth of ultrathin Ga and Ga–N films on the surface of a single-crystal silicon substrate Si(111). The spectrum of 3-keV He^+ ions scattered at an angle of $\theta = 135°$ from the surface of a Ga–N film with a thickness of 3.3 monolayers is shown in Fig. 11 [187]. In this study, a linear dependence of the He^+/Ga scattering peak half-width on the thickness of a gallium surface coating was discovered in the range of 1–9 monolayers. Monitoring the change in the He^+/Ga and He^+/Si scattering peak heights made it possible to conclude that the growth pattern of the gallium layers was close to the 'layer plus islet' regime.

The LEIS method is used to optimize production processes in state-of-the-art microelectronics (see, for example, [188, 189] and references therein). Study [188] showed the potential of this method for controlling the nucleation, growth, and diffusion of ultrathin HfO_2 and TiN films, which play an important role in complementary metal–oxide–semiconductor (CMOS) technology. Based on the analysis of scattering spectra, information was obtained on nucleation and final formation of thin-film gates in field-effect transistors, and the relationship of these data with the electrical characteristics and reliability of the transistors was found. In [189], experimental LEIS studies of ultrathin bilayer structures Si (1.7 nm, 4.3 nm, 6 nm)/W (20 nm) and Si (1.6 nm)/Mo (20 nm) were carried out along with computer modeling of the LEIS spectra. It was found that this approach makes it possible to obtain information on hidden interfaces without layer-by-layer sputtering of samples.

We now return to the feasibility of conducting chemical analysis using the LEIS method with the registration of ion yield oscillations depending on the energy (velocity) of the primary ions. Table 1 [96] presented in Section 2.2.1 provides a list of elements for which such oscillations have been detected (class II). For primary He^+ ions, there are only 9 such elements, and all of them have filled d-electron shells. In [99], it was shown that the chemical state of In atoms affects the amplitude and shape of the oscillation peaks, i.e., the probability P^+ that scattered helium ions preserve their charge.

Figure 12a [99] shows $\eta(E_0)$ graphs plotted for pure indium and indium contained in various chemical compounds. It is evident that, depending on the chemical environment of the In atoms, the $\eta(E_0)$ curves differ, although not very significantly. The data presented in Fig. 12a were processed using the fast Fourier transform (FFT), and the spectral analysis results are presented in Fig. 12b. The differences among the shapes and amplitudes of the oscillation peaks became more noticeable. Similar results using FFT were obtained for the scattering of He^+ ions from the surface of nonconducting chemical compounds of Pb and Bi [101]. In fact, these are all the experimental data known to us regarding the influence of the chemical (electronic) state of the surface atoms of elements classified as class II [96] on the intensity of He^+ scattering peaks from such atoms.

Can LEIS be used in practice for chemical analysis in this case? In our opinion, the answer is negative. First, the number of elements in class II with oscillatory dependences is very small — only 9 for primary He^+ ions. Second, and most importantly, these are fairly heavy elements (Ga and heavier) with a relative mass of $\alpha \gg 1$. For such elements, the mass resolution in He^+ ion scattering is very low, i.e., the overlap (interference) of scattering peaks from elements with similar masses is quite significant, which can lead to distortion of oscillatory dependences when analyzing chemical compounds. Table 1 [96] indicates that ion yield oscillations were also found for Ne^+ ions scattered from gallium atoms, which improves the situation with mass spectral resolution. However, one of the authors of the review (A.B. Tolstoguzov) used the energy-mass analysis mode to show that, when Ne^+ is scattered from pure Ga and In samples in the energy range $E_0 = 0.4$–2.2 keV [109] and from $A^{III}B^V$ semiconductor compounds (GaP, GaAs, InP, and InAs) in the energy range $E_0 = 0.6-1.6$ eV [110] at a scattering angle $\theta = 120°$, ion yield oscillations were not observed. It is worth noting that only energy-mass analysis can provide reliable results for heavy primary ions, the interaction of which with the surface of the samples under study is accompanied by noticeable sputtering.

Thus, studies of the oscillatory dependence of ion yield on primary ion energy are of interest in fundamental research for a deeper understanding of neutralization processes in ion scattering. For practice, the dependence of ion yield on the chemical environment, i.e., the influence of matrix effects, is undesirable, as it may distort the results of quantitative analysis using the LEIS method. As an example, we can cite the results of studies of He^+ ion scattering ($E_0 = 1$–3.5 keV) from the surface of various graphite samples [104], which showed that, due to the influence of matrix effects, a quantitative assessment of the carbon concentration is only possible provided additional information on the chemical state of its atoms is available.

We conclude this section with a brief review of publications on the application of LEIS in the USSR and Russia. As mentioned earlier, most of the basic studies of ion scattering were carried out at universities and academic research centers (Moscow State University, Moscow Aviation Institute, Moscow Engineering Physics Institute, Leningrad Polytechnic Institute, Ioffe Institute, Research Nuclear Physics Institute of Moscow State University, etc.) and were aimed at

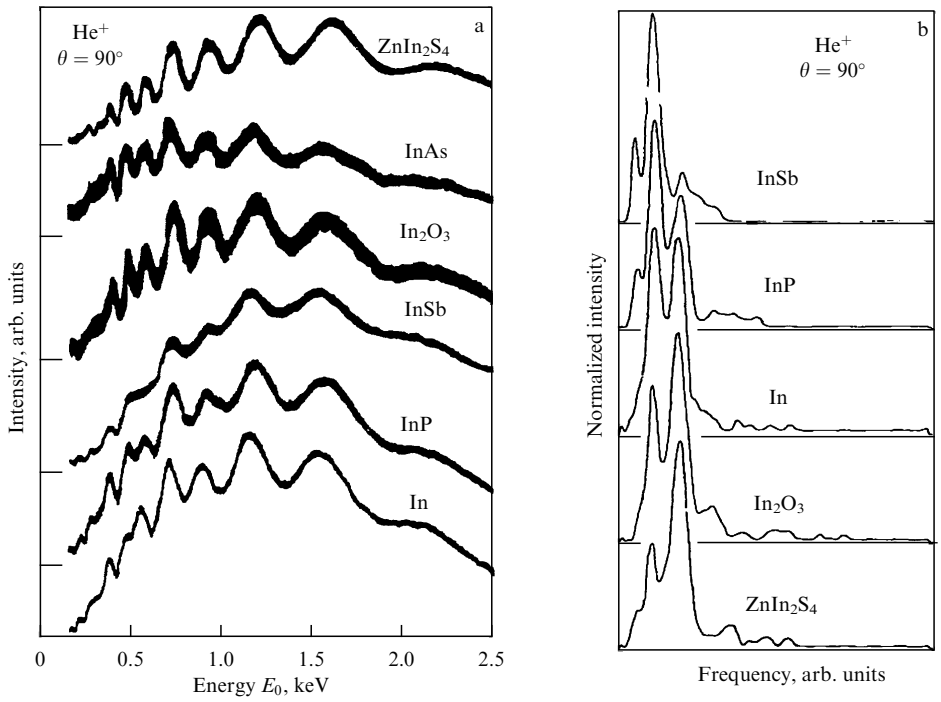

Figure 12. (a) Experimental oscillation dependences $\eta(E_0)$ for He^+ ions ($E_0 = 0.2-2.5$ keV, $\theta = 90°$) scattered from surface of pure indium and its chemical compounds. (b) Plots of spectral density of yield, obtained after processing experimental oscillation dependences using FFT method [99].

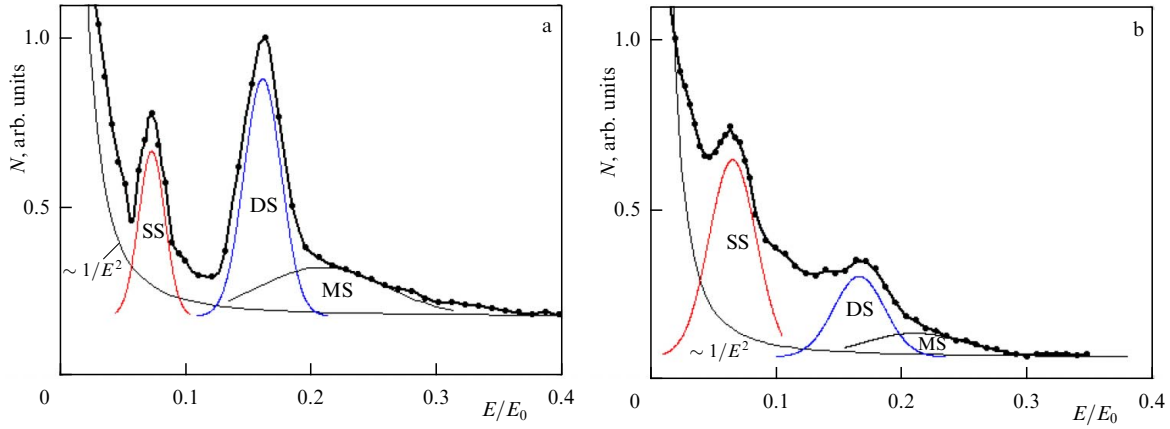

Figure 13. Energy spectrum of positive ions emitted during bombardment of surface of (a) pure Ge and (b) $Si_{1-x}Ge_x$ ($x = 5.8\%$) solid solution with Ar^+ ions with energy $E_0 = 4$ keV: SS is single scattering peak, DS is double scattering peak, and MS is multiple scattering peak of Ar^+/Ge. Background was subtracted from spectra according to inverse-square dependence on energy of emitted ions [196].

research, theoretical studies, and computer modeling of neutralization processes, multiple scattering, determining interaction potentials, and the influence of the structure of single-crystal surfaces on the energy and angular distributions of scattered ions (see, for example, [43–45, 60–64, 119, 124] and references therein). Among the applied studies, those carried out in the 1980s and early 1990s at NITI (Ryazan, USSR) can be noted. Studies of thermionic emitters [47–49] and metallic alloys [50] have been mentioned above. Also noteworthy are the studies of $A^{III}B^{V}$ semiconductor compounds, including the analysis of the surface structure of InP(100) single-crystal samples by ion scattering and recoil atom methods [190] and the study of the elemental composition and surface stoichiometry of GaAs epitaxial layers, undoped and doped with an isovalent Sb impurity [191]. A recently published review [192] summarizes the results of the studies conducted at NITI in the 1980s and early 1990s that examined the surface of various thermionic emitters, including oxide, scandate, thoriated tungsten, and carbide cathodes, using ion and electron spectroscopy, including low-energy ion scattering.

Applied research was also conducted by Kurnaev's group at MEPhI. Described in [193] is a setup based on an ion monochromator for studying the interaction of plasma with the surface of plasma device materials using the LEIS method; results of an analysis of the composition of stainless steel and graphite using primary He^+ and Ar^+ ions with energies of $E_0 = 2-8$ keV are presented. In studies of water vapor adsorption on a W surface [194], a method for monitoring the thickness of the adsorbed layer was developed and the elemental composition of the surface layers was determined, while Ref. [195] describes a simple method for estimating the survival probability of He^+ ions reflected from the surface of various metals using binary collision codes.

We now focus on study [196], in which the double scattering effect was used to determine the Ge cluster content in an $Si_{1-x}Ge_x$ solid solution with a low Ge content ($x = 5.8\%$). To avoid the significant background associated with single Ar^+/Si scattering, an experimental geometry with an emitted ion detection angle of 129 degree relative to the primary beam incidence direction was chosen.

Figure 13a shows the reference energy spectrum of positive ions emitted from pure Ge upon bombardment of a sample with an Ar^+ ion beam with an energy $E_0 = 3$ keV. The spectrum exhibits distinct peaks of double (DS) and single (SS) scattering of Ar^+ ions by Ge atoms. To the right of the double scattering peak, a background (denoted by MS) associated with multiple collisions is observed.

Figure 13b shows the energy spectrum of positive ions measured by bombarding an $Si_{1-x}Ge_x$ sample ($x = 5.8\%$) with Ar^+ ions with an energy $E_0 = 4$ keV. The intensity ratio of the double to single scattering peaks I^+_{DS}/I^+_{SS} for the $Si_{1-x}Ge_x$ solid solution and pure Ge, $\{I^+_{DS}/I^+_{SS}(Si_{1-x}Ge_x)\}/\{I^+_{DS}/I^+_{SS}(Ge)\} = 0.19 \pm 0.02$, allows one to estimate the number of Ge atoms present in the solid solution as clusters. The proposed technique using double scattering of argon ions offers unique sensitivity for determining the fraction of clusters in solid solutions.

4.2 Analytical capabilities of fast recoil spectroscopy

Returning to Fig. 2, we see that, during an elementary scattering event, the target atom M acquires kinetic energy E_2 as a result of an elastic collision, the value of which can be calculated using Eqn (2). Under certain experimental conditions (relative mass α, incidence angles β, and departure angles ψ), the mass of this atom, called the fast recoil atom, can be determined from the measured energy spectra, provided that it leaves the target surface in an ionized state and has not lost part of its kinetic energy due to elastic and inelastic collisions with other target atoms and the electron gas.

By analogy with Eqn (5), we obtain [197]

$$M = M_0\left(2\gamma^2 - 1 \pm \gamma\sqrt{\gamma^2 - 1}\right), \qquad (16)$$

where $\gamma = \sqrt{E_0/E_2}\cos\psi$.

It should be immediately noted that calculations using Eqn (16) involve ambiguity in determining the recoil atom mass: the same peak with energy E_2 can belong to either a surface atom with mass $M < M_0$ or $M > M_0$. To unambiguously determine the recoil atom mass, it is necessary to use heavy primary ions. Another option is to use two types of primary ions with different masses, for example, Ne^+ and Ar^+, either concurrently or sequentially.

We now briefly discuss the options for using fast recoil atoms for surface analysis. The method underlying such studies is called Direct Recoil Spectrometry (DRS) [198], and, in combination with LEIS, Scatterings And Recoiling Spectrometry (SARS) [199]. In Russian-language scientific publications, the abbreviation DRS is used, although

attempts have been made to call this method RAS (recoil atom spectrometry) (spektroskopiya atomov otdachi, SAO) [197, 200]. The DRS method is similar to SIMS, mentioned in Section 1 of this review. However, while slow sputtered ions, which provide information in SIMS, undergo multiple collisions with atoms in the near-surface layer before leaving the target surface and 'forget' their initial position and charge state, recoil atoms emerge from virtually the same position they occupied at the moment of collision with the primary ion. Therefore, by analyzing their energy and angular distributions, it is possible to determine the surface structure with high accuracy [201, 202] and examine the adsorption of various gases, including hydrogen and its isotopes [203, 204]. It must be taken into account that recoil atoms can leave the target surface both in the ionized state and as neutral particles (in the ground or excited state). Assuming that the charge state of recoil atoms does not alter during knockout by the primary ion and upon departure from the target surface, by measuring their energy spectra, including those of neutral particles, we can obtain information about the charge state of adsorbed atoms.

We now consider the use of the terms 'spectroscopy' and 'spectrometry' in the names of diagnostic methods. Why, for example, is there the term low-energy ion scattering spectroscopy but recoil atom spectrometry, or X-ray photoelectron spectroscopy but secondary ion mass spectrometry? The authors failed to find a clear explanation for these differences in either the Russian or English-language scientific literature. For example, [205] explains that "spectroscopy studies the interaction of electromagnetic radiation with matter, while spectrometry deals with the measurement of specific spectra." The IUPAC Compendium of Chemical Terminology [206] asserts that the terms *spectroscopy* and *spectrometry* are often used interchangeably, but there are subtle differences between them. Specifically, *spectroscopy is the study of physical systems using the electromagnetic radiation with which they interact or which they produce, while spectrometry is the measurement of such radiation as a means of obtaining information about the systems and their components*.

4.3 Determining particle–surface interaction potential

In [207], by modeling the energy spectra of hydrogen atoms backscattered from a gold surface at various emission angles β, measured in [208], data on the particle–surface interaction potential for the H–Au system were obtained. By varying the parameters of the interaction potential, good agreement with experiment was achieved, and the result was independent of the analytical form of the potential used.

As can be seen from Fig. 14, the obtained values of the potential for the particle–surface case differ significantly from the DFT (density functional theory) potential for the gas phase [75]. The screening constant is increased by 10–15%. In [209], a formula was proposed that takes into account the change in screening due to the presence of electrons in the metal, which agrees well with experiment:

$$U(R) = \frac{Z_1(Z_2 - N_2)}{R} \exp\left(-\frac{R}{R_D}\right) + \frac{Z_1 N_2}{R} \times \sum_{i=1}^{3} A_i \exp\left(-B_i \frac{R}{a}\right) \exp\left(-\frac{R}{R_D}\right), \quad (17)$$

where Z_1 and Z_2 are the nuclear charges of the colliding atoms, N_2 is the number of bound electrons of the lattice ion,

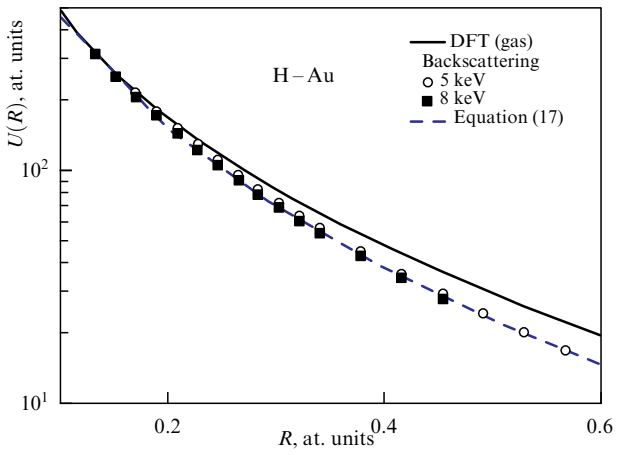

Figure 14. Comparison of interaction potential $U(R)$ obtained by simulation of backscattering (symbols) for initial energies of 5 and 8 keV with DFT potential obtained for gas phase [75]. Dashed line is calculation using Eqn (17).

R_D is the Debye screening length [210] (for gold $R_D = 1.358$ au), A_i and B_i are the expansion coefficients in the Molière potential [76], and a is the screening constant ($a = 0.8853 a_B Z_2^{-1.2} N_2^{0.87}$, $a_B = 0.529$ Å).

The formulas obtained are recommended for use in the analysis of ion scattering on metal targets.

4.4 Determining surface structure and characteristics

4.4.1 Surface structure analysis. Low-energy ion backscattering has been successfully used to analyze surface crystalline structures. A detailed description can be found in monographs [4, 8, 39, 40, 43–45, 57–59] and the aforementioned articles and reviews [42, 60–64, 191, 201, 202].

Note that low-energy electron diffraction, a method often used for surface structure analysis, fails to determine the elements to which the atoms being studied belong. This requires the use of an additional method, such as Auger or photoelectron spectroscopy.

We now present several examples of structural analysis using the LEIS method, which, as noted above, exhibits elemental sensitivity to the uppermost (visible) surface layer.

Figure 15 [211, 212] shows the change in the intensity of the scattered signal of 2-keV Ne^+ ions when scanning the surface of a Pt[110] crystal along the azimuthal angle δ. The minimum intensity corresponds to signal blocking during scattering along closely packed crystalline directions, which allows reconstructing the crystal surface structure. Interpretation of these spectra using computer modeling provides comprehensive information on the crystallographic structure of the surface. It should be noted that the recorded signal is associated exclusively with ion scattering on the surface monolayer. This allows the study of surface relaxation and surface restructuring during coating application.

Figure 16 [211, 213] presents the results of scanning the surfaces of silicon monohydride and dihydride crystals with 2-keV Ne^+ ions at the azimuthal angle δ. As can be seen from Fig. 16, the technique allows one to analyze the structure and position of hydrogen atoms with varying target composition.

In many cases, the neutral component is dominant in ion scattering, and the use of the time-of-flight technique enables

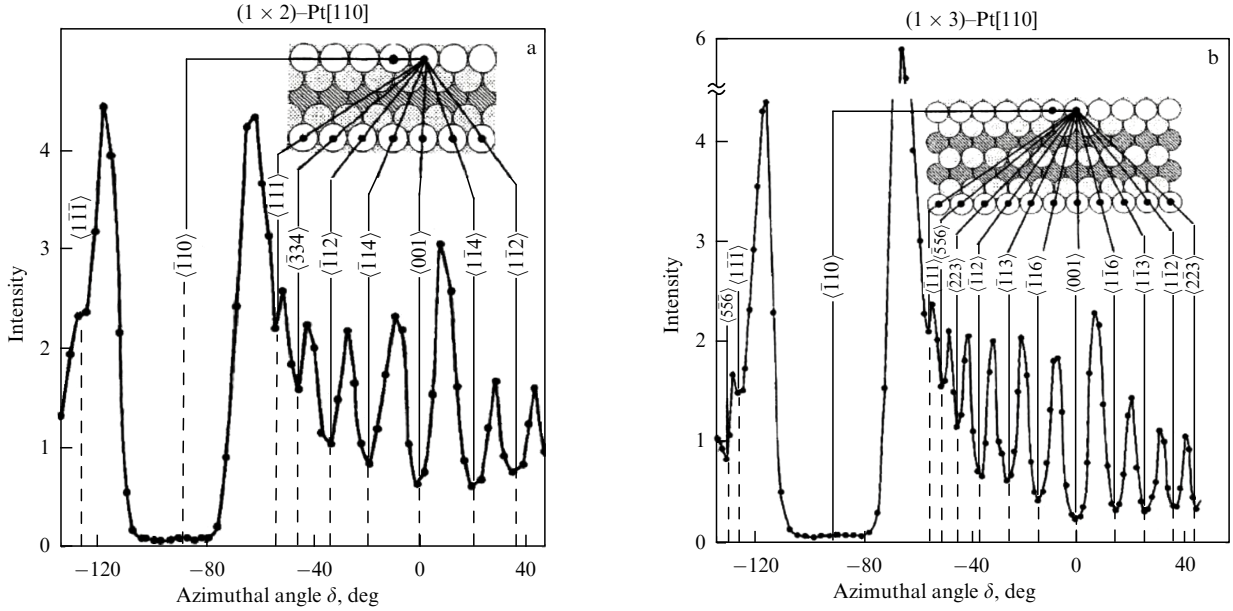

Figure 15. Scattering intensity of 2-keV Ne^+ ions as function of azimuthal angle δ for Pt[110] in reconstructed phases: (a) (1 × 2), (b) (1 × 3). Scattering angle $\theta = 28°$ and incidence angle $\beta = 6°$ [211, 212].

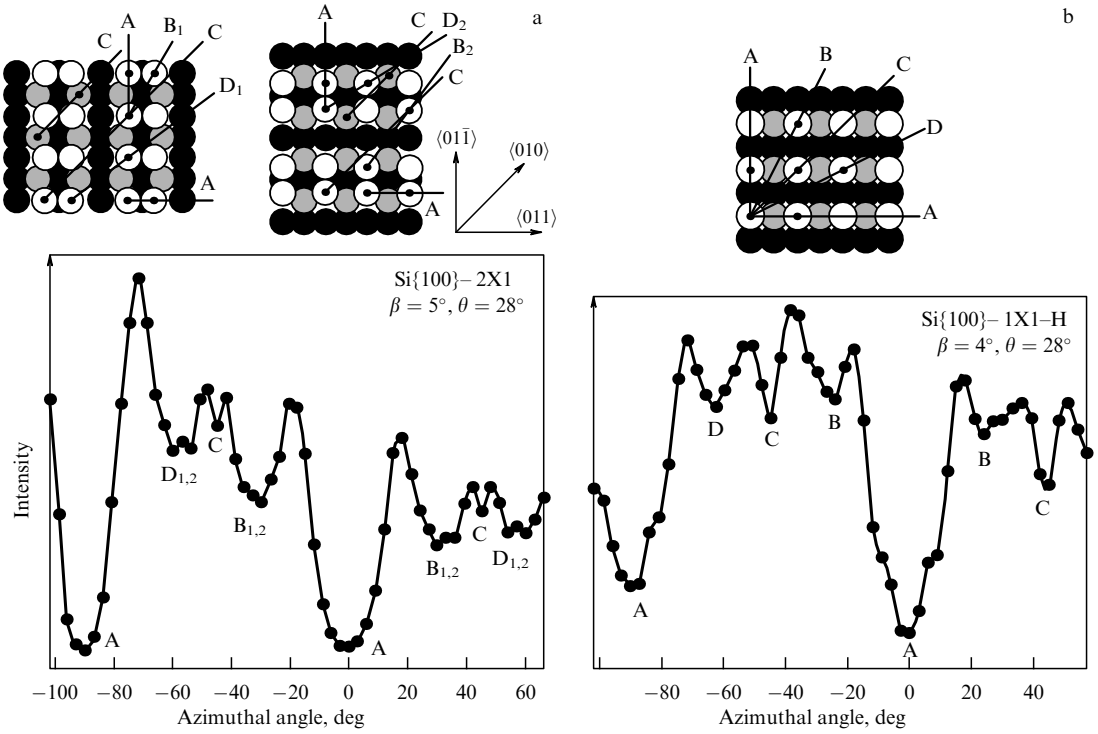

Figure 16. Signal intensity of hydrogen recoil atoms knocked out from surface of Si{100} crystal as function of azimuthal angle δ for phases: (a) monohydride (2 × 1) – H, (b) dihydride (1 × 1) – H. Intensity minima in figures are identified in accordance with layer structure of figures given above, in which hydrogen atoms are designated by small dark dots [211, 213].

recording the energy spectra of scattered neutral atoms. TOF spectra are more easily modeled using computer codes such as MARLOWE [133] and SARIC [136]. An example of using the SARIC program to model the scattering spectra of argon and recoil atoms during bombardment of a clean and oxygen-coated Ni(111) surface can be found in [214], and the results of computer modeling and experimental data on helium scattering from an Ni(110) surface are presented in [215–217]. Agreement between the computer simulation results and the experimental data was very good.

Measurement of the ion fraction of scattered ions as a function of the scanning angle was also used to study the surface structure [218]. Depending on the coverage of the cadmium sulfide crystal surface with Cd or S atoms, the observed pattern altered significantly.

We note study [190], which examined the angular distributions of scattered ions and ionized recoil atoms during irradiation of the surface of an InP(100) crystalline target with 3-keV Ne^+ ions. It was found that indium atoms are predominantly located in the upper layer of the target, and

these atoms can shift from positions corresponding to the (1×1) structure to positions more consistent with the (4×2) structure predicted in [219].

A method using scattering from two target atoms at an angle close to 180° was proposed for studying the surface structure in [220, 221]. This method is called Impact Collision Ion and Neutral Scattering Spectroscopy (ICISS/NICISS). The use of time-of-flight techniques made it possible to study the shadowing effect of a surface atom on the scattering of an underlying atom.

The ICISS/NICISS method allows one to determine the position of each surface atom and conduct a quantitative analysis of the surface composition and structure. It analyzes not only the outer surface layer but also the subsurface atomic layers and the dynamic processes occurring on the surface and within these layers.

To summarize this section, we note that the use of low-energy ion scattering and fast recoil atoms in combination with computer modeling is an effective way to obtain information about the crystallographic structure of a surface.

4.4.2 Using rainbow scattering to determine surface parameters. Rainbow scattering of ions/atoms is a process in which particles scattered from a target surface deviate from a straight trajectory at various angles, forming a 'rainbow' of scattered particles (see, e.g., [222] and references therein). It should be noted that, as early as 1967, V.E. Yurasova and colleagues [45, 223] observed the 'rainbow' effect for the trajectories of ions captured in the channeling mode with transition to adjacent channels.

In [224], the scattering of argon atoms from the surface of Al and Ag crystals was studied at grazing angles of incidence along the crystal axes. A structure related to the focusing of beam atoms on the atoms of the surface half-channel was observed in the dependences of the intensity of scattered particles on the azimuthal angle φ. In this case, multiple scattering of atoms occurs at grazing angles of incidence, and the central peak obtained in [224] was associated with scattering along the central axis of the channel at $\varphi = 0$. For two parallel rows of aluminum atoms forming a surface half-channel, the impact parameter p is the same, i.e., the scattering angle is not a monotonic function of the impact parameter. A maximum appears on the $\varphi(p)$ dependence, leading to a rainbow scattering effect at angle φ_r.

Computer modeling of particle trajectories taking into account multiple scattering predicts the presence of sharp peaks at angles φ_r. Thermal motion of target atoms broadens these peaks, making it possible to determine the oscillation amplitude of the surface atoms, which turn out to be 0.010 ± 0.002 nm for Ar–Ag and 0.0123 ± 0.0007 nm for Ar–Al.

Modeling the dependence of the position of the angle φ_r on the collision energy E_0 enabled determining the parameters of the interaction potential for the cases under consideration. As can be seen from Fig. 17, a significant difference is observed between the obtained potential and conventional models of potentials for collisions in the gas phase. In [226], this difference is explained by the induction of the incident particle imaging potential in the metal.

The rainbow scattering effect of K^+ ions on a W(110) surface was observed in [227] at incident ion energies below 50 eV. In [228], 3D modeling of the scattered particle trajectories was carried out, and the potential parameters were determined. The modeling also took into account the induced imaging potential of the incident ion–metal surface system.

5. Scattering of inert gas ions in hyperthermal energy range

As noted in Section 1, the primary E_0 ion energy in the LEIS method is typically limited from below by a value of approximately 300–500 eV. This limitation is due to a decrease in the yield of scattered ions (see Fig. 8) and the difficulty of obtaining a primary ion current sufficient for an acceptable level of analytical sensitivity. A fundamental issue is the cutoff energy of primary ions, below which the spectra of scattered ions can no longer be interpreted in the binary elastic collision (BEC) model.

Study [229] found that, for the scattering of He^+ and Ne^+ ions from a copper surface, the BEC cutoff energy is 40 and 20 eV, respectively. It should be noted that such energies, commonly referred to as hyperthermal, span a range from a few to hundreds of eV. The authors of [229] used a sector magnetic mass spectrometer with a Nir ionization source

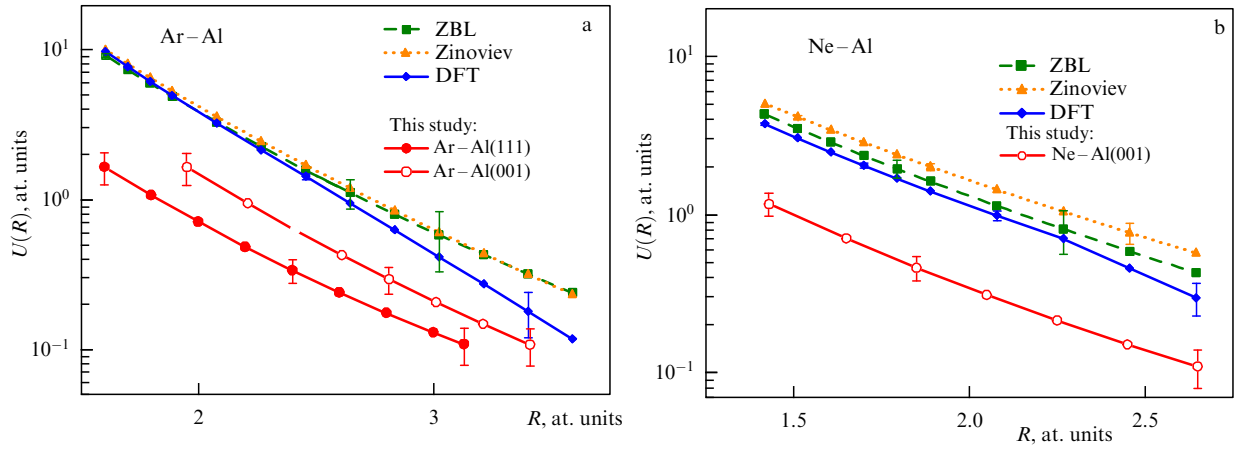

Figure 17. Potentials of particle–surface interaction as a function of interatomic distance: (a) for Ar–Al(111) and Ar–Al(001), (b) for Ne–Al(001). Solid line with circles represents potential obtained by fitting calculated spectra to experimental ones. Other lines show calculations for ZBL [67], Zinoviev [73], and DFT [75] potentials.

[230] to calibrate the energy/mass of the detected ions. This simplified version of energy-mass analysis made it possible to separate the peaks of scattered, secondary sputtered, and desorbed ions, which is especially important in the hyperthermal energy range. Later, in [231, 232], when studying the scattering of He^+ and Ne^+ ions at an angle of $\theta = 135°$ from the surfaces of Au, Bi, Pb, and InAs, it was shown that the BEC model 'is operative' up to energies of 1.5–2 eV. Note that, in these studies, only an energy analysis of the detected ions was used.

The applicability of the binary elastic collision model for the scattering of Ne^+ and Ar^+ ions at an angle of $\theta = 90°$ from the surfaces of various materials was more thoroughly tested in [233]. Primary ions were generated in an inductively coupled plasma (ICP) source with subsequent mass filtration by a 60° sector magnetic separator, and the scattered ions were detected in the energy-mass analysis mode using a 90° electrostatic deflector and a quadrupole mass filter.

The generalized results of the studies in the form of the dependence of the kinematic factor K_1 (see Eqn (1)) on the relative mass $\alpha = M/M_0$ for primary ion energies $E_0 = 50-1000$ eV, i.e., including the hyperthermal energy range, has shown that, for almost all the targets studied, from aluminum to lead, fairly good agreement was observed between the calculated and experimental values of the kinematic factor K_1. This indicates the validity of the binary elastic collision model up to an energy of 50 eV. The authors of [233] noted that, for primary ion/surface atom combinations with coefficient α close to 1 (Ne^+/Al and Ne^+/Si), inelastic energy losses were observed; therefore, the upper limit of E_0 for these targets was limited to 500 eV, and the experimental values of K_1 turned out to be somewhat lower than the calculated ones.

The number of publications devoted to the scattering of inert-gas ions in the hyperthermal energy range is fairly small due to the complexity of conducting experiments at such energies. A detailed review of these activities for the period up to 2001 can be found in [234]. Of the more recent ones, one can note the already mentioned publication by M.J. Gordon et al. [233] and other studies conducted in his group, which examined inelastic energy losses of Ne^+ during scattering from the surface of various metals [235, 236]. The hyperthermal energy range is also of interest in studying the scattering of molecular ions [237] and alkali metals, including computer modeling (see, for example, [238] and references therein).

In general, it can be concluded that the correctness of the BEC approximation for describing the scattering processes of inert gas ions in the hyperthermal energy range, at least up to energies of 30–50 eV, is proven. At the same time, some studies, for example [239, 240], have shown that the scattering peak shifted toward energies higher than those predicted by Eqn (1). The authors of these studies, a detailed analysis of which can be found in [234], considered such a shift to be a manifestation of the nonbinary (multiparticle or collective) nature of the interaction of primary ions with the surface. According to this concept, surface atoms in collisions with the primary ion are considered to be bound to each other, and, for a correct mathematical description of the scattering event, it was proposed to introduce an effective mass into Eqn (1), i.e., the mass of a hypothetical surface formation $M_{\text{eff}} = nM$, where n is the total number of surface atoms with mass M involved in the scattering process. This approach was initially proposed by Veksler [241] to describe the scattering of alkali metal ions (K^+, Rb^+, and Cs^+) with energies $E_0 = 100$–300 eV from the surface of refractory metals W and Mo, and was subsequently applied by many researchers (see, e.g., [13]). In [242], based on an analysis of published data and computer modeling, it was concluded that, at energies below 30 eV, the scattering of atomic particles, including noble gas ions, occurs from a complex of surface atoms with an effective mass M_{eff}.

From a theoretical point of view, a deviation from the binary nature of collisions should be observed when the time of interaction of the incident particle with a surface atom becomes comparable to the oscillation period of this atom, and the energy of the colliding particles is close to the binding energy of the atoms on the surface, i.e., is several eV [8, 243]. These conditions are satisfied for $\alpha \ll 1$, i.e., when the mass of the incident particle M_0 is much greater than that of the surface atom M, and for a scattering angle exceeding $\theta_{\max} = \arcsin\alpha$ (see Eqn (6)).

A question arises as to the existence of a boundary energy of incident particles, above which backscattering processes can be interpreted in the binary elastic collision model, and below which only as a collective (multiparticle) interaction; otherwise, can both approximations 'be operative' concurrently in a certain energy range? If this is true, then two peaks may be observed concurrently in the spectrum of scattered ions, the energy position of one of which being described by the BEC model, and that of the second, by a collective interaction involving the effective mass of surface atoms.

Two such peaks were first experimentally observed in study [225], which was already referenced in this review. The energy of the second peak, called the focal peak, was close to the energy of the primary E_0 ions, and it was hypothesized that its appearance is the "reflection of incident ions from close-packed atomic chains, the direction of which coincides with (or is close to) the recoil momentum from which the ion is reflected" [231]. The effective mass was not mentioned in this study, but the proposed explanation is essentially close to this concept.

In [234], the spectra of $^{20}Ne^+$ ions scattered from the surface of polycrystalline Au and Pt samples were measured in the energy-mass analysis mode, which is presented in detail in Section 6.1. The measurements were carried out with primary ion energies $E_0 = 40-1000$ eV at scattering angle $\theta = 120°$ and incidence angle $\beta = 60°$. The dynamics of changes in the $^{20}Ne^+$/Au scattering spectra as a function of E_0 can be traced in Fig. 18 [234], in which intensity is presented on a logarithmic scale normalized to the maximum intensity of the peaks. Up to an energy of 100 eV, the spectra only contain two peaks, designated as the SP peak of neon ions implanted in the sample and then sputtered, and the BEC peak of binary elastic collisions of $^{20}Ne^+$/Au. With a further decrease in E_0, a third peak appears, which is designated in Fig. 18 as HE, a high-energy peak. The position of the maximum of this peak is close to the energy of the primary ions, and its relative intensity increases with decreasing E_0.

Measurements of the dependence of the kinematic factor K_1 on the energy of primary ions E_0 for the BEC and HE peaks showed in [234] that, for the BEC peak, the experimental values of K_1 virtually coincided with the calculated ones up to energies $E_0 = 70$–80 eV, while, for the HE peak, they were close to 1. It is worth noting that the HE peak was observed in the spectra only after prolonged bombardment of the sample surface with Ne^+ ions (1 keV/1 μA, 60 min, dose of about 10^{16} cm^{-2}).

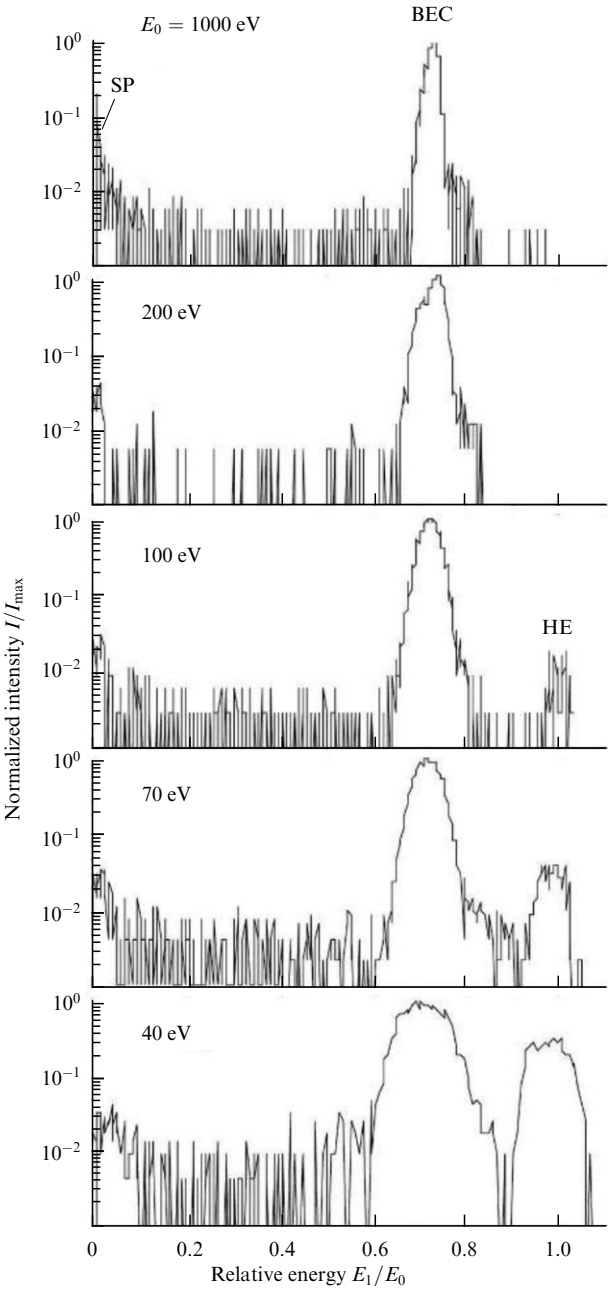

Figure 18. Normalized spectra of $^{20}Ne^+$ ions scattered from surface of Au sample, measured at $E_0 = 40-1000$ eV and scattering angle $\theta = 120°$ and incidence angle $\beta = 60°$: SP is peak of sputtered neon ions, BEC is peak of binary elastic collisions, and HE is high-energy peak [234].

Also in [234], an attempt was made to detect the HE peak for primary He^+, Ne^+, and Ar^+ ions in scattering from other targets, including polycrystalline samples of Cu, Ag, Pt, and Ta metals and single-crystal samples of Si and GaP semiconductors. In addition to the $^{20}Ne^+/Au$ combination, peaks with energies close to E_0, but with low intensity, were only observed for $^4He^+/Au$ and $^{20}Ne^+/Pt$ at energies below 50 eV. To clarify the nature of the HE peak, various instrumental factors and physical processes that could have caused the appearance of such a peak were considered and analyzed (a detailed review can be found in [234]). It was ultimately concluded that, when a gold sample's surface is irradiated with neon ions, some of the primary ions are scattered as a result of binary elastic collisions (the BEC peak), while the other portion interacts with a group of atoms, for example, with a surface cluster consisting of n gold atoms (the HE peak). Using Eqn (5) with effective mass M_{eff} of the interacting surface atoms yields an n value of about 10–15 for $^{20}Ne^+/Au$. It is known in [244] that gold atoms can form planar ($n \leqslant 10$) and tetrahedral ($10 < n < 20$) clusters, many of which are highly stable. The authors of [245], who were the first to observe the existence of two peaks in the spectrum of scattered ions, also ultimately arrived at a cluster model for the interaction of hyperthermal energy ions with the surface.

The effective mass does not fully explain the nature of the HE peak, especially since only the ion fraction of the reflected particles is measured. It is possible that the ion scattering kinematics remain unaltered for all primary ion/surface atom combinations studied in [234], including those for which the HE peak was not detected, but the decrease in the ion-survival probability P^+ of scattered ions with decreasing primary ion energy prevented this peak from being detected.

Concluding this section, it should be noted that studying the patterns of ion scattering in the hyperthermal energy range is not only of theoretical interest but also of great practical importance for understanding the processes of plasma interaction with the wall of a fusion reactor, the development of ion-beam deposition technology for thin films, reactive etching, precision polishing of semiconductor wafers with a cluster ion beam, etc.

6. Some promising areas for development of LEIS method

6.1 Energy-mass analysis

Backscattering is far from the only or primary process occurring during the interaction of noble gas ions in the 0.5–5-keV energy range with solid surfaces. Even for light He^+ ions, in addition to scattering, sputtering (erosion) of the surface under the action of the ion beam is observed, although the sputtering efficiency is insignificant, $k_{sp} \sim 0.1$ atom/ion [184]. This is one of the reasons why the vast majority of LEIS studies have been and continue to be carried out using helium ions. However, as shown earlier in Section 2.1, the mass spectral resolution of the LEIS method, i.e., the separation of He^+ ion scattering peaks from surface atoms with similar masses in the range above 30 amu, becomes problematic and requires the use of heavier primary ions, such as neon and argon. In this case, surface sputtering becomes more significant ($k_{sp} \sim 1$ atom/ion) [184], and the contribution of sputtered secondary ions to the observed energy spectra can no longer be ruled out by simply subtracting the exponentially decaying background, as was done, for example, in [56, 246].

Figure 19 displays the energy spectra of scattered Ne^+ ions and sputtered secondary Al^+ ions obtained by A.B. Tolstoguzov during bombardment of the surface of a polycrystalline aluminum target with 3-keV Ne^+ ions. The figure shows that the spectrum of Ne^+ ions is almost completely covered by the spectrum of Al^+ ions. Therefore, the use of heavy primary ions in LEIS, especially when analyzing the surface of samples containing atoms with M masses close to those of the primary M_0 ions, requires additional mass separation of the recorded particles. Time-of-flight mass spectrometers (TOF-MSs) fail to separate scattered and sputtered secondary ions, as they assume that all analyzed particles have either the same mass or the same energy.

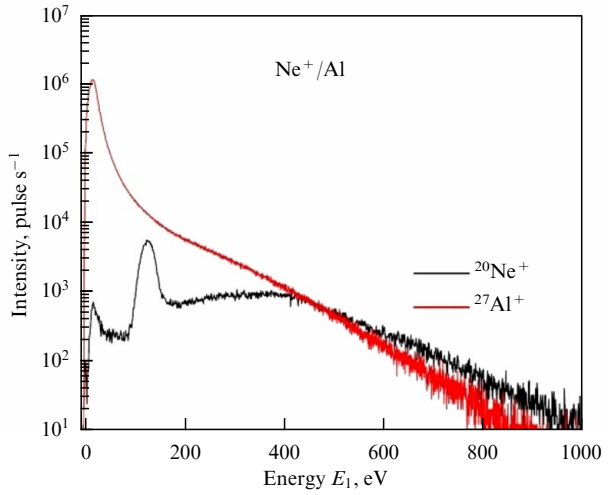

Figure 19. Energy spectra of scattered $^{20}Ne^+$ ions and sputtered secondary $^{27}Al^+$ ions obtained by bombarding polycrystalline aluminum target with Ne^+ ions ($E_0 = 3$ keV, $\theta = 120°$, $\beta = 60°$).

The first experiments on energy-mass analysis of scattered ions were carried out as early as the 1970s [247, 248]. In [247], a 90° prism electrostatic energy analyzer and a quadrupole mass filter tuned to the primary ion mass were used to this end, while in [248], a sector magnetic mass spectrometer was employed as the mass analyzer. It is important to note that study [247] was the first to demonstrate the advantages of combining LEIS and SIMS. Previously, as indeed now, especially in the studies conducted by Brongersma's group, the basic element of LEIS spectrometers was and remains the energy analyzer, and surface sputtering and the resulting secondary ions are considered artifacts (errors) that must be suppressed. This approach remains dominant in LEIS, although attempts have been made to combine a sector electrostatic energy analyzer with a time-of-flight mass spectrometer [249]. Pulse modulation of the primary Ar^+ beam was used, and the scattering angle was chosen equal to 47°, which made it possible to analyze not only scattered and secondary sputtered ions, but also fast recoil atoms.

Wittmaack, a recognized authority in the field of ion sputtering and secondary ion emission (see, for example, [178]), returned to the idea of energy-mass analysis of scattered ions. He proposed using the abbreviation MARISS (Mass Resolved Ion Scattering Spectrometry) as the name for this method [89]; in the Russian version, it is called mass-separated ion scattering [244]. The experiments were carried out on the DORAMIS setup [89], equipped with a plasma source of primary ions, an electrostatic energy filter, and a quadrupole mass spectrometer.

In this study, the energy spectra of scattered Kr^+ isotope ions and sputtered secondary $^{93}Nb^+$ ions were measured in the MARISS mode by bombarding a polycrystalline niobium target with Kr^+ ions ($E_0 = 10$ keV, $\theta = 135°$, $\beta = 90°$). The intensity of sputtered niobium ions was shown to significantly exceed that of scattered krypton ions, the energy spectra of which could not be recorded without mass separation. A peak of krypton ions with an energy close to zero was also observed. These krypton ions were initially implanted in the target under study and then sputtered by the primary ion beam.

In the same study, the inelastic energy losses Q were measured for the Ar^+/Ti and Kr^+/Nb combinations and found to be 90 and 250 eV, respectively, while for doubly charged Ne^{2+} ions formed by scattering of singly charged Ne^+ ions from a silicon target, the value $Q = 120 \pm 15$ eV was obtained (see also Section 2.4). Using the multi-isotope method for the determination of surface concentration, the neutralization constant value $v_c = 1.5 \times 10^4$ m s^{-1} was also determined for krypton ions scattered from a niobium surface. Compared to the dual-isotope determination method initially proposed in [88], where the surface of the sample under study was sequentially bombarded with isotopic helium ions (see Section 2.2.1), in the MARISS method, all isotopic ions simultaneously irradiated the surface, which enhanced the measurement accuracy.

Wittmaak applied the MARISS method together with SIMS in a depth profiling analysis of a silicon target consisting of isotopically pure ^{28}Si and ^{30}Si layers [251] and in studies of the surface of SiO_2 samples cleaned by ion sputtering and Si samples oxidized in an oxygen stream [252]. In the aforementioned studies, the main advantages of the energy-mass analysis of scattered ions (MARISS method) were formulated and experimentally confirmed. Compared to the energy analysis alone (LEIS method), they are: (1) elimination of the interference between scattered and secondary sputtered ions, (2) suppression of the background from doubly and multiply charged scattered ions, (3) use of a primary ion beam consisting of different types of ions, including isotopic ones. We discuss below these advantages in more detail, including those related to depth profiling analysis with ion beam sputtering of the surface and concurrent detection of signals from scattered and secondary sputtered ions.

While in his studies [89, 251, 252] Wittmaak continued and developed the hardware approach proposed in [247] in the configuration including an electrostatic energy analyzer and quadrupole mass spectrometer, in [253], the idea was revived to use a modified Cameca IMS-3f sector magnetic mass spectrometer for energy-mass analysis of scattered ions, similar to what was done in [248].

In this instrument, the potential of the sample U_s was varied (scanned) during recording of the energy distributions of scattered and secondary sputtered ions, and the energy of the scattered ions E_1 was calculated as

$$E_1 = E_{pass} - eU_s\,, \tag{18}$$

where E_{pass} is the fixed transmission energy of the energy analyzer, equal to 4.5 keV.

It should be noted that the energy of the argon ions emitted by the ion source was $E_i = 12.5$ keV, but, since the sample potential U_s varied during the recording of spectra, the energy of these ions E_0 upon interaction with the surface is

$$E_0 = E_i - eU_s\,. \tag{19}$$

Furthermore, the scattering angle θ, which was 42.4° at a fixed sample potential of $U_s = 4.5$ keV, also changed with the sample potential. The position of the primary ion beam on the sample surface also changed $\Delta\theta$ (formulas describing such changes can be found in [253]). Given the above, it is understandable why the use of magnetic mass spectrometers for the energy-mass analysis of scattered ions has not undergone further development. To our knowledge, the authors of [253] published only one other article [254], where they presented the results of studies of the scattering of alkali metal ions $^{133}Cs^+$ and $^{39}K^+$ from the surfaces of metal targets Ta, Au, and Cu.

The MARISS method in combination with SIMS was used in studies by one of the authors of this review (A.B. Tolstoguzov) during his work at the CNR-IENI research center (Padua, Italy) from 1998 to 2003. The main element of the experimental setup was a modified EQS 1000 mass-energy analyzer, developed by Hiden (UK) [255] for studying plasma processes. A detailed description of the EQS 1000 operation in MARISS mode can be found in [256, 257].

Located at the input of the instrument are an extractor with a single lens and an ionizer with an electron source designed for residual gas analysis (RGA) and neutral particle ionization operating in secondary neutral mass spectrometry (SNMS) mode. The design of the extractor and the grounded shielding electrode was modified, since the EQS was originally intended only for plasma analysis, and in MARISS/SIMS mode with a fixed sample potential, the efficiency of ion collection and transmission by the extractor significantly decreased. To this end, the electric fields and trajectories of scattered and sputtered ions were numerically modeled in the energy range from 0 to 1000 eV using the SIMION 3D program.

Energy analysis of scattered and sputtered ions was carried out using a 45° cylindrical deflector with a system of quadrupole electrostatic lenses, and a quadrupole filter was employed for mass spectral analysis. Ions were detected using a channel electron multiplier offset from the analyzer axis. The energy analyzer operated in constant transmission mode across the entire energy range of the analyzed ions, and at a transmission energy of $E_{\text{pass}} = 80$ eV, its energy resolution did not exceed $\Delta E_a = 3$ eV (FMHW). The mass resolution of the quadrupole filter was $\Delta M = 0.75$ amu (FWHM) in the analyzed mass range of 0.5–250 amu. An IQE 12/38 ion gun [143] was used as a source of primary inert gas ions (He^+, Ne^+, Ar^+), and the scattering angle in MARISS mode was $\theta = 120 \pm 2°$.

The mass-energy analyzer was controlled and the experimental results were processed using the EQS MASsoft program [255, 256], which provided flexible control of the instrument by selecting various operating modes (MARISS, SIMS, RGA). The potentials on the main functional units were optimized using autotuning to obtain the maximum intensity of the recorded signals, and the graphical interface facilitated scanning and measuring various experimental parameters, such as energy, mass, and sample current. Up to 300 scans and various measurements could be conducted in a single cycle.

Figure 20 [257] displays the spectra of Ar^+ ions with an energy of $E_0 = 2$ keV scattered at angle $\theta = 120°$ from the surface of a polycrystalline La sample. In Figure 20a, the spectrum was obtained in the energy analysis mode (LEIS) with a linear intensity scale, while in Fig. 20b, it was measured in the energy-mass analysis mode (MARISS) with a logarithmic intensity scale.

In Figure 20a, only two peaks are visible: a low-energy one associated with sputtering of the lanthanum surface by argon ions, and the elastic single scattering peak of Ar^+/La. The data presented in Fig. 20b are much more informative. It turns out that the low-energy peak includes three peaks of secondary sputtered atomic and molecular ions, namely $^{139}La^+$, $^{16}O^+$, $^{155}(LaO)^+$, and a peak of $^{40}Ar^+$ ions implanted from the primary ion beam into the lanthanum sample and then sputtered. Regarding the scattered ions, Fig. 20b shows the $^{40}Ar^+$/La spectrum with a peak of elastic single scattering from La atoms on the surface and an intense background of re-ionized argon ions scattered from lanthanum atoms in the near-surface layers of the sample and having undergone inelastic energy losses. Also observed is a peak of elastic scattering of doubly ionized $^{40}Ar^+$/La ions, which is completely 'covered' by the spectrum of re-ionized scattered argon ions.

As noted in Section 2.4, the MARISS method was used in study [123] to measure inelastic energy losses Q during scattering of isotopic ions $^{20}Ne^+$ and $^{22}Ne^+$ from aluminum and silicon targets and also to obtain Q values for doubly charged neon ions formed during scattering of singly charged neon ions from the surface of these targets. In [90], using the method of two-isotope determination with the concurrent use of primary ions $^{20}Ne^+$ and $^{22}Ne^+$ (ion current ratio $^{22}I_0/^{20}I_0 = 0.102$), the values of the neutralization constant v_c for neon ions in the energy range of 0.5–1.5 keV were obtained during scattering from the surface of polycrystalline samples of Cu, Ag, Au, and Pt. They turned out to be 2.05×10^5 m s^{-1} (Cu), 2.15×10^5 m s^{-1} (Ag), 1.90×10^5 m s^{-1} (Au), and 1.67×10^5 m s^{-1} (Pt). It should be noted that, for the copper subgroup metals, the v_c values were approximately the same and larger in magnitude than those of platinum, the mass of whose atoms differed slightly from that of gold atoms, but with different electron filling of the d-band.

The results of MARISS measurements of the spectra of $^{20}Ne^+$ ions in the energy range of 0.4–1.96 keV scattered from the surface of single-crystal GaP (100) samples [250] can also

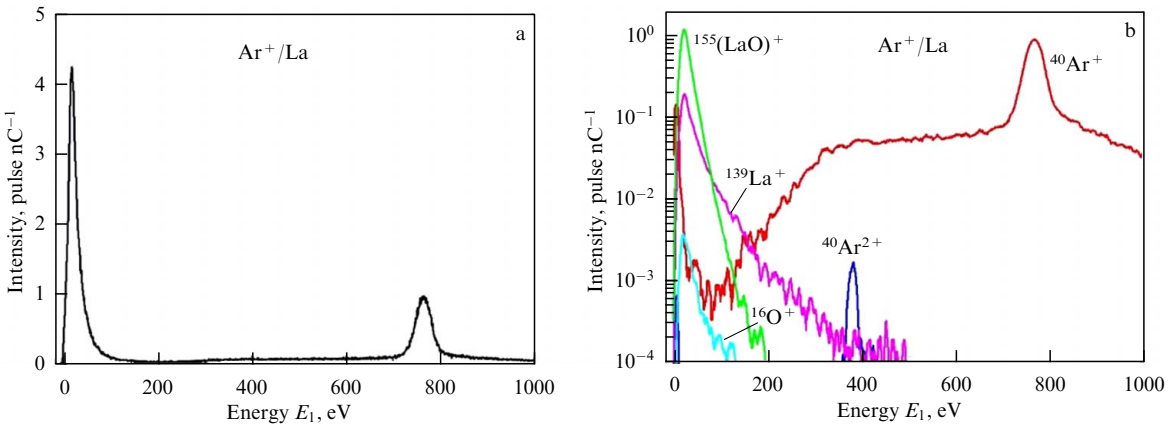

Figure 20. Spectrum of scattered and sputtered ions obtained by bombarding lanthanum sample with 2-keV Ar^+ ions: (a) energy analysis mode (LEIS), (b) energy-mass analysis mode (MARISS) [257].

be noted. It was found that these spectra contain not only the Ne^+/P and Ne^+/Ga scattering peaks along with the peak of sputtered neon ions, but also a broad peak ('bump'), the energy position of which weakly depends on the energy of the primary E_0 ions. This peak became noticeably pronounced at $E_0 > 1$ keV, and the main contribution to its intensity was made by re-ionized neon ions that had undergone multiple collisions with gallium and phosphorus atoms on the surface and in deeper layers of the sample.

Medieval Venetian dinars from the era of Doge Dandolo were studied in [258] using the LEIS method in the energy-mass analysis mode (MARISS). Detailed information on these studies can be found in monograph [259]. The aim of the study was to determine the quantitative composition of the surface and near-surface region of the silver billon alloy from which the dinars were made. The coins have great cultural value, so the research method could not damage their surface. Measurements were carried out on an experimental setup with an EQS 1000 mass energy analyzer. For the analysis in the MARISS mode and concurrent layer-by-layer sputtering, $^{20}Ne^+$ ions ($E_0 = 1$ keV, $\theta = 145°$) were used with a sample current of 1 μA. Preliminary quantitative calibration was carried out using pure samples of copper, silver, and gold, of which the billon alloy consists.

The spectra of neon scattering from the calibration samples are presented in Fig. 21a, and Fig. 21b displays typical concentration profiles of Ag, Cu, and Au obtained by depth profiling analysis of the near-surface region of the dinars. Figure 21b shows that the surface is enriched in silver (up to 80 at.%), the concentration of which decreased deeper into the samples. The copper concentration increased, while the gold content remained virtually constant (at 5 at.%) throughout the entire studied dinar depth.

Depth profiling analysis in MARISS mode can be carried out with a 'mixed' ion beam consisting of helium and neon or argon ions. This approach makes it possible to virtually simultaneously record $^4He^+$ scattering peaks from light elements such as carbon, nitrogen, and oxygen and from heavier elements such as $^{20}Ne^+$ or $^{40}Ar^+$ ions, which also effectively sputter the surface and provide higher mass resolution than helium ions. Furthermore, in MARISS mode, with the necessary software available, it is also possible to observe secondary ion mass peaks, i.e., combine ion scattering (MARISS) with secondary ion mass spectrometry (SIMS). Examples of combined MARISS-SIMS depth profiling analysis are contained in [260, 261].

6.2 Ion microscopy

In this section, we briefly consider the use of backscattered ion methods and instrumentation in state-of-the-art ion microscopes. We discuss the Zeiss ORION NanoFab ion microscope [262], equipped with a strongly focused gas field ion source (GFIS) of helium ions (GFIS [263]). The external appearance of the ion microscope is displayed in Fig. 22a, while Fig. 22b schematically depicts the vacuum chamber with the ion source, a sample, and a silicon drift ion detector [264, 265].

Secondary electrons generated by the interaction of He^+ ions with the sample allow obtaining a high-contrast topographic image of the surface with a lateral resolution at the nanometer level. For elemental analysis, it was proposed to use helium ions and neutral atoms scattered from atoms in the near-surface layers of the sample [264–266]. It is worth noting that the energy of helium ions in ion microscopes is $E_0 = 10-40$ keV, which is higher than the energy range of primary ions in LEIS, but lower than in MEIS instruments (see Section 1). In addition, the ion beam is focused to a minimum diameter of 0.25 nm. Under these conditions, the primary ions penetrate the sample deeper than the surface layer, losing part of their energy E_0 to the excitation of electrons before the event of elastic scattering on the sample atoms. Scattered ions also deposit part of their energy E_1 as they move toward the sample surface. Taking into account the above, a SPECTRA cooled silicon drift detector [267] with an energy resolution of about 4.5 keV and a detection threshold energy of 10 keV was used in [264, 265] to detect scattered ions.

To enhance the energy resolution when detecting scattered ions, a time-of-flight method with pulse modulation of the primary ion beam was used [266]. Figure 23 [266] shows the spectrum of 30-keV He^+ scattered from the surface of a 2-nm-thick HfO_2 layer on a silicon substrate. The time resolution was 17.3 ns with a total detected charge of 1.9 nC. The time scale was calibrated using the ion-photon emission peak, also shown in Fig. 23 [266].

In the ion scattering mode, a lateral resolution of 54 nm was achieved using the TOF method. Further studies aim at implementing a correlation microscopy mode with concur-

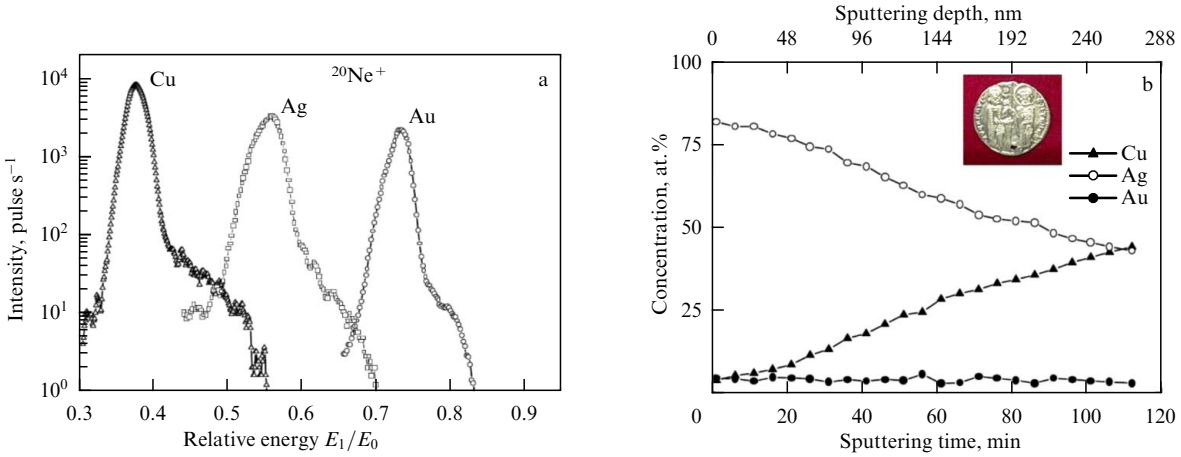

Figure 21. (a) Combined spectra of $^{20}Ne^+$ ions ($E_0 = 1$ keV, $\theta = 145°$) scattered from surface of Cu, Ag, and Au calibration samples; (b) concentration profiles of Cu, Ag, and Au obtained by depth profiling analysis of near-surface region of dinars [258].

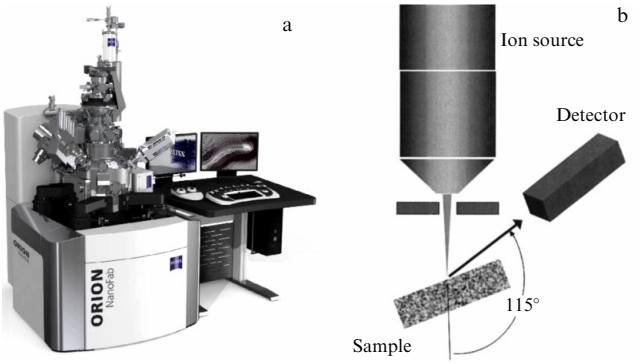

Figure 22. External view of Zeiss ORION NanoFab ion microscope (a) and schematic representation of vacuum chamber with ion detector (b) [264, 265].

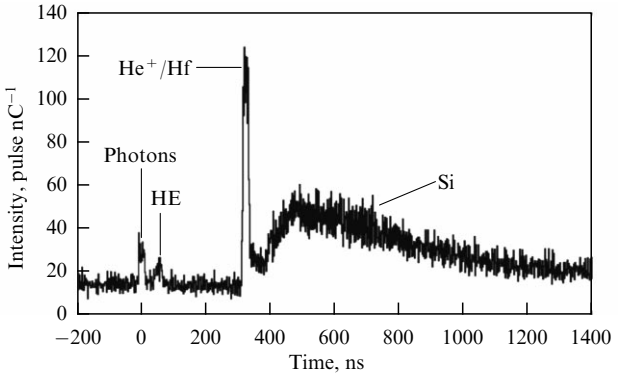

Figure 23. Time-of-flight spectrum of scattered ions measured by irradiating a 2-nm-thick HfO_2 layer on surface of silicon substrate with 30-keV He^+ ions.

rent recording of secondary electron, scattered, and secondary sputtered ion images, which will enable obtainment of information about the elemental composition and topography of the studied objects at the nanoscale.

Concluding the microscopy section, we dwell on study [268], which examined the surface reconstruction of single-crystal magnetic Fe_4N samples using low-energy backscattered ions and fast ionized recoil atoms and scanning tunneling microscopy (STM) [53]. The measurements were carried out on an experimental STM setup equipped with a pulsed Ar^+ ion source and a time-of-flight detector for recording the spectra of scattered ions and fast ionized recoil atoms. The time resolution of the TOF detector was 200 ns, and the scattering angle was $\theta = 54°$ at an incidence angle of $\beta = 12°$. Recording such spectra improved the quality of STM image interpretation due to more accurate determination of the positions of atoms on the sample surface by comparing the measured and simulated angular distributions of scattered ions and ionized recoil atoms.

7. Conclusions

The authors of this review, based on their experience in experimental and theoretical research in the development of analytical instrumentation for ion beam surface analysis and ion-surface interactions, have sought to provide a comprehensive analysis of the basic and applied aspects of low-energy ion scattering. Section 4 focuses on studies of liquid surfaces, nanoparticles, and clusters and modern materials and devices for micro- and nanoelectronics. Computer programs for modeling ion/atom interactions with surfaces, crystallographic structure studies, determination of the particle–surface interaction potential, and rainbow scattering studies are also considered. The application of ion scattering in state-of-the-art ion microscopes is discussed. Particular attention is given to the scattering of heavy ions (neon and argon) in the low- and hyperthermal-energy ranges and the energy-mass analysis of scattered and secondary sputtered ions as promising methods for developing surface diagnostics.

In practical terms, the future of the LEIS method is seen in applications to the analysis of liquid surfaces, including ionic liquids, polymeric and organic materials, static and dynamic depth profiling analysis of ultrathin films and various coatings, the creation of effective catalysts and corrosion inhibitors, elemental and structural analysis of clusters, and the development of fusion reactors. The use of ion scattering in ion microscopes for elemental analysis with high spatial resolution is very promising. In terms of basic research, the hyperthermal energy range below 100 eV is of great interest, as two models operate simultaneously: binary elastic collisions and collective (multiparticle) interactions. Worthy of attention is the study of the dependence of the ion yield on the energy of primary ions, which can provide information on the electronic state (chemical composition) of the uppermost surface layer. Studies of the energy and angular distributions of recoil atoms in the ionized and neutral states will allow the position of these atoms on the surface to be determined with high accuracy.

It is worth emphasizing once again that the LEIS method features unique sensitivity to the elemental composition and structural features of the uppermost surface layer, allowing quantitative interpretation of the results. Many LEIS studies have been conducted in conjunction with electron and X-ray photoelectron spectroscopy. In the opinion of the authors of the review, the combination of LEIS with secondary ion mass spectrometry (SIMS) in the form of energy-mass analysis appears to be a promising direction for the development of this method. From a basic-research perspective, the underlying duality of the ion scattering method is noteworthy.

On the one hand, the elementary scattering event and the energy position of the scattering peaks are considered in the binary elastic collision model and classical mechanics, while the processes of charge preservation by the scattered ion, i.e., the intensity of the signal from scattered ions, are primarily interpreted in quantum mechanical models of interactions with electrons in solids.

Progress in the development of the LEIS method is based not only on the results of basic research and computer modeling, in which Soviet and Russian researchers remain leaders, but also on the hardware employed in this technique.

In the final stages of review preparation, the authors became aware of recent publications by Russian scientists from MEPhI, in which the LEIS method was successfully applied to the analysis of materials of interest for fusion research [269–271]. The authors believe that it is essential to deploy production of state-of-the-art surface diagnostic equipment, including LEIS, in Russia. This factor is crucial for the successful development of micro- and nanoelectronics and ion-beam-based methods of material modification in Russia.

Acknowledgments. A.B. Tolstoguzov is grateful to his scientific adviser, G.N. Shuppe, for proposing studies in the

ion scattering method; to E.S. Mashkova, V.A. Molchanov, and A.M. Borisov for their interest in and support of his research; and to all his colleagues from his joint work at NITI (Ryazan, USSR) and the CNR-IENI research center (Padua, Italy) for their assistance in conducting experiments, processing experimental data, and preparing scientific publications and reports.

References

1. Descartes R *Regulae ad directionem ingenii (Rules for the Direction of the Understanding): An Early Manuscript Version* (Oxford: Oxford Univ. Press, 2023); in Russian: Descartes R "Pravila dlya rukovodstva uma" ("Rules for the direction of the mind"), in *Sochineniya* (Essays) (Moscow: Mysl', 1989); https://gtmarket.ru/library/basis/3958
2. Brongersma H H et al. *Surf. Sci. Rep.* **62** 63 (2007)
3. Brongersma H H et al. *Vacuum* **84** 1005 (2010)
4. Mashkova E S, Molchanov V A *Primenenie Rasseyaniya Ionov dlya Analiza Tverdykh Tel* (Application of Ion Scattering for the Analysis of Solids) (Moscow: Energoizdat, 1995)
5. Volkov S S, Tolstoguzov A B *Spektroskopiya Obratno Rasseyannykh Ionov Nizkikh Energii* (Low-energy Ion Backscatter Spectroscopy) (Obzory po Elektronnoi Tekhnike. Ser. 7. Tekhnologiya, Organizatsiya Proizvodstva i Oborudovenie (Electronic Engineering Reviews. Ser. 7. Technology, Production Organization, and Equipment), No. 15(820)) (Moscow: TsNII Elektronika, 1981) 79 pp.
6. Gainullin I K *Phys. Usp.* **63** 888 (2020); *Usp. Fiz. Nauk* **190** 950 (2020)
7. van der Veen J F *Surf. Sci. Rep.* **5** 199 (1985)
8. Mashkova E S, Molchanov V A *Medium-Energy Ion Reflection from Solids* (Modern Problems in Condensed Matter Sciences, Vol. 11) (Amsterdam: North-Holland, 1985); Translated from Russian: *Rasseyanie Ionov Srednikh Energii Poverkhnostyami Tverdykh Tel* (Moscow: Atomizdat, 1980)
9. Shemukhin A A et al. *J. Surf. Investig.* **7** 318 (2013); *Poverkhnost', Rentgen., Sinkhrotron., Neitron. Issled.* (4) 25 (2013)
10. Shipatov E T *Obratnoe Rasseyanie Bystrykh Ionov, Teoriya, Eksperiment, Praktika* (Backscattering of Fast Ions. Theory, Experiment, Practice) (Rostov-on-Don: Izd. Rostov. Gos. Univ., 1988)
11. Mayer J W, Rimini E (Eds) *Ion Beam Handbook for Material Analysis* (New York: Academic Press, 1977)
12. Overbury S H *Nucl. Instrum. Meth. Phys. Res. B* **27** 65 (1987)
13. Evstifeev V V *Mnogochastichnye Vzaimodeistviya pri Rasseyanii Medlennykh Ionov Poverkhnost'yu Metalla* (Multiparticle Interactions during Scattering of Slow Ions by a Metal Surface) (Penza: Izd. Penzenskogo Gos. Univ., 2009)
14. Maazouz M et al. *Surf. Sci.* **398** 49 (1998)
15. Kuehner J A, Almovist E, Bromley D A *Phys. Rev.* **131** 1254 (1963)
16. Tolstoguzov A B, Gusev S I, Fu D J *Tech. Phys. Lett.* **48** (4) 36 (2022); *Pis'ma Zh. Tekh. Fiz.* **48** (7) 47 (2022)
17. Arifov U A, Ayukhanov A Kh *Dokl. Akad. Nauk Uzbek. SSR* (4) 12 (1951)
18. Eremeev M A *Dokl. Akad. Nauk SSSR* **79** 775 (1951)
19. Panin B V *Sov. Phys. JETP* **15** 215 (1962); *Zh. Eksp. Teor. Fiz.* **42** 313 (1962)
20. Benninghoven A, Rüdenauer F G, Werner H W *Secondary Ion Mass Spectrometry. Basic Concepts, Instrumental Aspects, Applications, and Trends* (New York: J. Wiley, 1987)
21. Smith D P *J. Appl. Phys.* **18** 340 (1967)
22. Goff R F, Smith D P *J. Vac. Sci. Technol.* **7** 72 (1970)
23. Smith D P *Surf. Sci.* **25** 171 (1971)
24. Smith D P, US Patent 3,480,744 dated Nov. 25 (1969)
25. Begemann S H A, Boers A L *Surf. Sci.* **30** 134 (1972)
26. Heiland W, Taglauer E *J. Vac. Sci. Technol.* **9** 620 (1972)
27. Brongersmal H H, Mu P M *Surf. Sci.* **35** 393 (1973)
28. Czanderna A W (Ed.) *Methods of Surface Analysis* (Amsterdam: Elsevier, 1975); Translated into Russian: *Metody Analiza Poverkhnosti* (Translated from English, Eds V V Korablev, N N Petrov) (Moscow: Mir, 1979)
29. Fiermans L, Vennik J, Dekeyser W (Eds) *Electron and Ion Spectroscopy of Solids* (New York: Plenum Press, 1978); Translated into Russian: *Elektronnaya i Ionnaya Spektroskopiya Tverdykh Tel* (Translated from English, Ed. V I Rakhovskii) (Moscow: Mir, 1981)
30. Briggs D, Seah M P (Eds) *Practical Surface Analysis: by Auger and X-ray Photoelectron Spectroscopy* (Chichester: J. Wiley and Sons, 1983); Translated into Russian: *Analiz Poverknosti Metodami Ozhei Rentgenovskoi Fotoelektronnoi Spektroskopii* (Translated from English, Eds V I Rakhovskii, I S Rez) (Moscow: Mir, 1987)
31. Woodruff D P, Delchar T A *Modern Techniques of Surface Science* (Cambridge: Cambridge Univ. Press, 1986); Translated into Russian: *Sovremennye Metody Issledovaniya Poverkhnostei* (Translated from English, Ed. V I Rakhovskii) (Moscow: Mir, 1989)
32. Parilis E S *Effekt Auger* (Auger Effect) (Tashkent: Fan, 1969)
33. Nemoshkalenko V V, Aleshin V G *Electron Spectroscopy of Crystals* (New York: Plenum Press, 1979); Translated into English: *Elektronnya Spektroskopiya Kristallov* (Kiev: Naukova Dumka, 1976)
34. Cherepin V T, Vasiliev M A *Metody i Pribory dlya Analiza Poverkhnosti* (Methods and Instruments for Surface Analysis) (Kiev: Naukova Dumka, 1982) Handbook
35. Cherepin V T *Ionnyi Mikrozondovyi Analiz* (Ion Microprobe Analysis) (Kiev: Naukova Dumka, 1992)
36. Petrov N N, Abroyan I A *Diagnostika Poverkhnosti s Pomoshch'yu Ionnykh Puchkov* (Surface Diagnostics Using Ion Beams) (Leningrad: Izd. Leningrad. Univ., 1977)
37. Shuppe G N *Diagnostika Poverkhnostei Elektronnymi, Ionnymi i Fotonnymi Zondami* (Surface Diagnostics with Electron, Ion and Photon Probes) Pt. 2 (Ryazan': Izd. Ryazan. Radiotekh. Inst., 1984)
38. Oura K et al. *Surface Science: an Introduction* (Berlin: Springer, 2003); Translated into Russian: *Vvedenie v Fiziku Poverkhnosti* (Moscow: Nauka, 2006)
39. Vickerman J C, Gilmore I S (Eds) *Surface Analysis*: *The Principal Techniques* (Chichester: J. Wiley, 2009)
40. The Surface Science Society of Japan (Ed.) *Compendium of Surface and Interface Analysis* (Singapore: Springer, 2018)
41. Erickson R L, Smith D P *Phys. Rev. Lett.* **34** 297 (1975)
42. Niehus H, Heiland W, Taglauer E *Surf. Sci. Rep.* **17** 213 (1993)
43. Kurnaev V A, Mashkova E S, Molchanov V A *Otrazhenie Legkikh Ionov ot Poverkhnosti Tverdogo Tela* (Reflection of Light Ions from the Surface of a Solid Body) (Moscow: Energoatomizdat, 1985)
44. Ryazanov M I, Tilinin I S *Issledovanie Poverkhnosti po Obratnomu Rasseyaniyu Chastits* (Surface Investigation by Particle Backscattering) (Moscow: Energoatomizdat, 1985)
45. Yurasova V E *Vzaimodeistvie Ionov s Poverkhnost'yu. Izbrannye Trudy* (Ion-Surface Interactions: Selected Works) (Moscow, 1999)
46. Kawano H *Prog. Surf. Sci.* **97** 1000583 (2022)
47. Aristarkhova A A, Volkov S S, Tolstoguzov A B *Elektron. Promyshlen.* (1–2) 41 (1979)
48. Volkov S S, Tolstoguzov A B *Elektron. Tekh. Ser. 1. Elektronika SVCh* (9) 25 (1981)
49. Tolstoguzov A B, Shuppe G N *Radiotekh. Elektron.* **27** 592 (1982)
50. Tolstoguzov A B *Metallofizika* (5) 85 (1982)
51. Bush W *Julchen* (München: Adamant Media Corp., 2001)
52. Monreal R C *Prog. Surf. Sci.* **89** 80 (2014)
53. Mironov V L *Osnovy Skaniruyushchei Zondovoi Mikroskopii* (Basics of Scanning Probe Microscopy) (Moscow: Tekhnosfera, 2004)
54. IONTOF GmbH, https://www.iontof.com/
55. Cushman C V et al. *Anal. Methods* **8** 3419 (2016)
56. Průša S et al. *Appl. Surf. Sci.* **657** 158793 (2024)
57. Rabalais J W *Principles and Applications of Ion Scattering Spectrometry*: *Surface Chemical and Structural Analysis* (Hoboken, NJ: J. Wiley and Sons, 2003)
58. Parilis E S et al. *Teoriya Rasseyaniya Atomov Srednikh Energii Poverkhnost'yu Tverdogo Tela* (Theory of Scattering of Medium-Energy Atoms by the Surface of a Solid) (Tashkent: FAN, 1987)
59. Parilis E S et al. *Atomic Collisions on Solid Surfaces* (Amsterdam: North-Holland, 1993)
60. Yurasova V E *Izv. Akad. Nauk SSSR. Ser. Fiz.* **28** 1470 (1964)
61. Yurasova V E, Brzhezinskii V A, Ivanov G M *Sov. Phys. JETP* **20** 313 (1965); *Zh. Eksp. Teor. Fiz.* **47** 473 (1964)
62. Yurasova V E, Shulga V I, Karpuzov D S *Canadian J. Phys.* **46** 759 (1968)
63. Yurasova V E et al. *Radiation Effects* **12** 175 (1972)

64. Martynenko Yu V *Radiation Effects* **20** 211 (1973)
65. *Atlas Spektrov Obratno Rasseyannykh Ionov Inertnykh Gazov* (Atlas of Backscattered Ion Spectra of Inert Gases) (Ryazan': NITI, 1986)
66. Bierman D J, Turkenburg W C, Bhalla C P *Physica* **60** 357 (1972)
67. Landau L D, Lifshitz E M *Mechanics* Vol. 1 (Oxford: Butterworth-Heinemann, 1976); Translated into English: *Mekhanika* Vol. 1 (Moscow: Nauka, 1988)
68. Torrens L M *Interatomic Potentials* (New York: Academic Press, 1972)
69. Lehmann C *Interaction of Radiation with Solids and Elementary Defect Production* (Amsterdam: North-Holland, 1977); Translated into Russian: *Vzaimodeistvie Izlucheniya s Tverdym Telom i Obrazovanie Elementarnykh Defektov* (Translated from English, Ed. G I Babkin) (Moscow: Atomizdat, 1979)
70. Firsov O B *Sov. Phys. JETP* **7** (2) 308 (1958); *Zh. Eksp. Teor. Fiz.* **34** 447 (1958)
71. Robinson M T, Torrens I M *Phys. Rev. B* **9** 5008 (1974)
72. Ziegler I F, Biersack J P, Littmark U *The Stopping and Range of Ions in Solids* Vol. 1 (New York: Pergamon Press, 1985)
73. Zinov'ev A N *Tech. Phys.* **53** 13 (2008); *Zh. Tekh. Fiz.* **78** 15 (2008)
74. Wilson W D, Haggmark L G, Biersack J P *Phys. Rev. B* **15** 2458 (1977)
75. Zinoviev A N, Nordlund K *Nucl. Instrum. Meth. Phys. Res. B* **406** 511 (2017)
76. Molière G *Z. Naturforsch. A* **2** 133 (1949)
77. Abrahamson A A *Phys. Rev.* **178** 76 (1969)
78. Andersen H H, Sigmund P, Risø Report No. 103 (1965)
79. Tsuneyuki S, Tsukada M *Phys. Rev. B* **34** 5758 (1986)
80. Sasaki M et al. *Nucl. Instrum. Meth. Phys. Res. B* **190** 127 (2002)
81. Shekhter Sh Sh *Zh. Eksp. Teor. Fiz.* **7** 750 (1937)
82. Hagstrum H D *Phys. Rev.* **96** 336 (1954)
83. Abroyan I A, Eremeev M A, Petrov N N *Sov. Phys. Usp.* **10** 332 (1967); *Usp. Fiz. Nauk* **92** 105 (1967)
84. Winter H *Phys. Rep.* **367** 387 (2002)
85. Hagstrum H D *Phys. Rev.* **96** 336 (1954)
86. Woodruff D P *Nucl. Instrum. Meth. Phys. Res.* **194** 639 (1982)
87. Bertrand P et al. *Surf. Sci.* **68** 108 (1977)
88. Ackermans P A J et al. *Surf. Sci.* **227** 361 (1990)
89. Wittmaack K *Surf. Sci.* **345** 110 (1996)
90. Tolstogouzov A et al. *Surf. Sci.* **466** 127 (2000)
91. Rabalais J W et al. *J. Chem. Phys.* **83** 6489 (1985)
92. Kasi S R et al. *Surf. Sci. Rep.* **10** 1 (1989)
93. Buck T M et al. *Phys. Rev. B* **48** 774 (1993)
94. Cortenraad R et al. *Appl. Surf. Sci.* **146** 69 (1999)
95. Rusch T W, Erickson R L *J. Vac. Sci. Technol.* **13** 374 (1976)
96. Rusch T W, Erickson R L, in *Inelastic Ion-Surface Collisions* (Eds N H Tolk et al.) (New York: Academic Press, 1977)
97. *24th Intern. Workshop on Inelastic Ion-Surface Collisions, IISC-24, September 10–15, 2023, Charleston, South Carolina*; https://sciencewebb.clemson.edu/iisc24/iisc-history/
98. Tolk N et al. *Phys. Rev. Lett.* **36** 747 (1976)
99. Christensen D L et al. *Chem. Phys. Lett.* **44** 8 (1976)
100. Helbig H F, Adelmann P J *J. Vac. Sci. Technol.* **14** 488 (1977)
101. Christensen D L et al. *Nucl. Instrum. Meth.* **149** 587 (1978)
102. Zartner A, Taglauer E, Heiland W *Phys. Rev. Lett.* **40** 1259 (1978)
103. Helbig H F, Orvek K J *Nucl. Instrum. Meth.* **170** 505 (1980)
104. Mikhailov S N, van den Oetelaar L C A, Brongersma H H *Nucl. Instrum. Meth. Phys. Res. B* **93** 210 (1994)
105. Goebl D et al. *J. Phys. Condens. Matter* **25** 485006 (2013)
106. Erickson R L, Smith D P, US Patent 3,9290,989 dated Nov. 18 (1975)
107. Vaníčková E, Průša S, Šikola T *Surf. Sci. Spectra* **30** 024201 (2023)
108. Vaníčková E, Průša S, Šikola T *Nucl. Instrum. Meth. Phys. Res. B* **553** 165385 (2024)
109. Tolstogouzov A et al. *Surf. Sci.* **531** 95 (2003)
110. Tolstogouzov A, Daolio S, Pagura C *Nucl. Instrum. Meth. Phys. Res. B* **217** 246 (2004)
111. Canário A R et al. *Phys. Rev. B* **71** 121401 (2005)
112. Hecht T et al. *Phys. Rev. Lett.* **84** 2517 (2000)
113. Taglauer E et al. *Phys. Rev. Lett.* **45** 740 (1980)
114. Borisov A G et al. *Phys. Rev. B* **54** 17166 (1996)
115. Gainullin I K *Surf. Sci.* **677** 324 (2018)
116. Romero M A, Iglesias-García A, García E A *Surf. Sci.* **721** 122070 (2022)
117. Koppers W R et al. *Phys. Rev. B* **57** 13246 (1998)
118. Heiland W, Taglauer E *Nucl. Instrum. Meth.* **132** 535 (1976)
119. Babenko P Yu, Mikoushkin V M, Shergin A P *Tech. Phys.* **50** 1617 (2005); *Zh. Tekh. Fiz.* **75** (12) 82 (2005)
120. Hagstrum H D, in *Inelastic Ion-Surface Collisions* (Eds N H Tolk et al.) (New York: Academic Press, 1977)
121. MacDonald R J, O'Connor D J *Surf. Sci.* **124** 423 (1983)
122. Bertrand P, Pierson E, Beuken J M *Nucl. Instrum. Meth. Phys. Res. B* **33** 396 (1988)
123. Tolstogouzov A, Daolio S, Pagura C *Surf. Sci.* **441** 213 (1999)
124. Babenko P Yu, Shergin A P *Tech. Phys.* **54** 958 (2009); *Zh. Tekh. Fiz.* **79** (7) 32 (2009)
125. Xu F et al. *Phys. Rev. A* **57** 1096 (1998)
126. Draxler M et al. *Phys. Rev. A* **68** 022901 (2003)
127. Markin S N et al. *Phys. Rev. B* **78** 195122 (2008)
128. LEIS Energy Calculator. Institut für Angewandte Physik. Technische Univ. Wien, https://www2.iap.tuwien.ac.at/www/surface/leis
129. SRIM — The Stopping and Range of Ions in Matter, http://srim.org
130. Robinson M T, Torrens I M *Phys. Rev. B* **9** 5008 (1974)
131. Yamamura Y, Kimura H *Surf. Sci.* **185** L475 (1987)
132. Robinson M, Torrens I *Phys. Rev. B* **9** 5008 (1974)
133. Robinson M T *J. Nucl. Mater.* **103** 525 (1981)
134. Mutzke A et al., SDTrimSP Version 7.00. IPP Report 2024-06 (Greifswald: IPP, 2024)
135. Shulga V I *Radiation Effects* **70** 65 (1983)
136. Bykov V et al. *Nucl. Instrum. Meth. Phys. Res. B* **114** 371 (1996)
137. Meluzova D S et al. *J. Surf. Investig.* **13** 335 (2019); *Poverkhnost'. Rentgen., Sinkhrotron., Neitron. Issled.* (4) 74 (2019)
138. Babenko P Yu et al. *Nucl. Instrum. Meth. Phys. Res. B* **406** 460 (2017)
139. Thompson A P et al. *Comput. Phys. Commun.* **271** 108171 (2022)
140. Karolewski M A *Nucl. Instrum. Meth. Phys. Res. B* **230** 402 (2005)
141. Johnson P R, Sosolik C E *Comput. Phys. Commun.* **280** 108479 (2022)
142. Solov'ev A V, Tolstoguzov A B *Sov. Phys. Tech. Phys.* **32** 580 (1987); *Zh. Tekh. Fiz.* **57** 953 (1987)
143. IQE 12/38 Wien Filter. SPECS Group, https://www.specs-group.com/specs/products/detail/iqe-1238-wien-filter/
144. Afanas'ev V P, Yavor S Ya *Elektrostaticheskie Energoanalizatory dlya Puchkov Zaryazhennykh Chastits* (Electrostatic Energy Analyzers for Charged Particle Beams) (Moscow: Nauka, 1978)
145. ESCALAB QXi XPS Microprobe. Thermo Fisher Scientific Inc., https://www.thermofisher.com/ru/ru/home/electron-microscopy/products/xps-instruments/escalab.html
146. Teodoro O M N D, Silva J A M C, Moutinho A M C *Vacuum* **46** 1205 (1995)
147. Volkov S S et al. *Elektron. Promyshlen.* (5) 42 (1987)
148. Kessel'man L A, Tomashevskii A G *Elektron. Promyshlen.* (11–12) 102 (1978)
149. McKinney J T, US Patent 4,117,322 dated Sept. 26 (1978)
150. Gisler E, Bas E B *Vacuum* **36** 715 (1986)
151. Brongersma H H et al. *Rev. Sci. Instrum.* **49** 707 (1978)
152. Hellings G J A et al. *Surf. Sci.* **162** 913 (1985)
153. Ackermans P A J et al. *Nucl. Instrum. Meth. Phys. Res. B* **35** 541 (1988)
154. Brongersma H H et al. *Nucl. Instrum. Meth. Phys. Res. B* **190** 11 (2002)
155. Schultz J A et al. *Nucl. Instrum. Meth. Phys. Res. B* **118** 758 (1996)
156. Schultz J A, Schmidt H K, US Patent 5,087,815 dated Feb. 11 (1992)
157. Linnarsson M K et al. *Rev. Sci. Instrum.* **83** 095107 (2012)
158. Sortica M A et al. *Nucl. Instrum. Meth. Phys. Res. B* **463** 16 (2020)
159. Brongersma H H et al. *Nucl. Instrum. Meth. Phys. Res. B* **142** 377 (1998)
160. Ackermans P A J, Krutzen G C R, Brongersma H H *Nucl. Instrum. Meth. Phys. Res. B* **45** 384 (1990)
161. Jacobs J-P et al. *J. Vac. Sci. Technol. A* **12** 2308 (1994)
162. Průša S et al. *Surf. Sci. Spectra* **27** 024201 (2020)
163. Wilson R G, Stevie F A, Magee C W *Secondary Ion Mass Spectrometry: a Practical Handbook for Depth Profiling and Bulk Impurity Analysis* (New York: J. Wiley and Sons, 1989)

164. Wilson R G *Int. J. Mass Spectrom. Ion Proces.* **143** 43 (1995)
165. Drozdov M N et al. *Thin Solid Films* **607** 25 (2016)
166. Zhao H et al. *IEEE J. Select. Topics Quantum Electron.* **31** 7900208 (2025) DOI:10.1109/JSTQE.2024.3456439
167. Karpuzov D S *Surf. Sci.* **45** 342 (1974)
168. Poelsema B, Verheij L K, Boers A L *Surf. Sci.* **133** 344 (1983)
169. Hecht D, Strehblow H-H *J. Electroanal. Chem.* **436** 109 (1997)
170. Welton T *Chem. Rev.* **99** 2071 (1999)
171. Mazarov P, Dudnikov V G, Tolstoguzov A B *Phys. Usp.* **63** 1219 (2020); *Usp. Fiz. Nauk* **190** 1293 (2020)
172. Yang P et al. *J. Chem. Phys.* **135** 034502 (2011)
173. Caporali S, Bardi U, Lavacchi A *J. Electron Spectrosc. Relat. Phenom.* **151** 4 (2006)
174. Villar-Garcia I J et al. *Chem. Sci.* **5** 4404 (2014)
175. Andersson G, Ridings C *Chem. Rev.* **114** 8361 (2014)
176. Kumar A, Andersson G G *Adv. Colloid Interface Sci.* **333** 103302 (2024)
177. Almeida R M et al. *J. Non-Cryst. Solids* **385** 124 (2014)
178. Wittmaack K, in *Sputtering by Particle Bombardment III. Characteristics of Sputtered Particles, Technical Applications* (Topics in Applied Physics, Vol. 64, Eds R Behrisch, K Wittmaack) (Berlin: Springer, 1991) p. 161, DOI:10.1007/3540534288_18; Translated into Russian: *Raspylenie pod Deistviem Bombardirovki Chastitsami III. Kharakteristiki Raspylennykh Chastits, Primeneniya v Tekhnike* (Eds R Behrisch, K Wittmaack) (Moscow: Mir, 1998)
179. Fujimoto T, Iiyama M, Nakamura T, European Patent EP 06 46 786 dated Sept. 29 (1993)
180. Quantitative top atomic layer characterisation. The Qtac. IONTOF GmbH, https://www.iontof.com/qtac-low-energy-ion-scattering-leis-surface-analysis.html
181. Bare S R et al. *Surf. Sci.* **648** 376 (2016)
182. Šik O et al. *Vacuum* **152** 138 (2018)
183. ARXPS, Depth Profiling, XPD. SPECS Group, https://www.specs-group.com/specsgroup/knowledge/methods/detail/arxps-depth-profiling-xpd/
184. Andersen H H, Bay H, in *Sputtering by Particle Bombardment I. Physical Sputtering of Single-Element Solids* (Topics in Applied Physics, Vol. 47, Ed. R Behrisch) (Berlin: Springer, 1981) p. 145, DOI:10.1007/3540105212_9; Translated into Russian: *Raspylenie Tverdykh Tel Ionnoi Bombardirovkoi I. Fizicheskoe Raspylenie Odnoelementnykh Tverdykh Tel* (Ed. R Behrisch) (Moscow: Mir, 1984)
185. Rousset J L, Renouprez A J, Cadrot A M *Phys Rev. B* **58** 2150 (1998)
186. Rafati A, ter Veen R, Castner D G *Surf. Interface Anal.* **45** 1737 (2013)
187. Kolíbal M et al. *Surf. Sci.* **566–568** 885 (2004)
188. Dittmar K et al. *Surf. Interface Anal.* **49** 1175 (2017)
189. Valpreda A et al. *J. Vac. Sci. Technol. A* **41** 043203 (2023)
190. Aristarkhova A A et al. *Pis'ma Zh. Tekh. Fiz.* **15** (19) 81 (1989)
191. Aristarkhova A A et al. *Pis'ma Zh. Tekh. Fiz.* **16** (2) 43 (1990)
192. Volkov S S, Kitaeva T I, Nikolin S V *J. Surf. Investig.* **18** 1233 (2024); *Poverkhnost'. Rentgen., Sinkhrotron., Neitron. Issled.* (10) 94 (2024)
193. Mamedov N V et al. *Bull. Russ. Acad. Sci. Phys.* **76** 683 (2012); *Izv. Ross. Akad. Nauk Ser. Fiz.* **76** 764 (2012)
194. Mamedov N V et al. *Vacuum* **148** 248 (2018)
195. Mamedov N V, Mamedov I M *Bull. Russ. Acad. Sci. Phys.* **84** 713 (2020); *Izv. Ross. Akad. Nauk Ser. Fiz.* **84** 863 (2020)
196. Babenko P Yu, Shergin A P *Tech. Phys. Lett.* **33** 377 (2007); *Pis'ma Zh. Tekh. Fiz.* **33** (9) 37 (2007)
197. Volkov S S, Rutkovskii S V, Tolstoguzov A B *Elektron. Promyshlen.* (10–11) 41 (1982)
198. Rabalais J W *Critical Rev. Solid State Mater. Sci.* **14** 319 (1988)
199. Rabalais J W *Science* **250** 521 (1990)
200. Volkov S S et al. *Elektron. Promyshlen.* (5) 42 (1987)
201. Borisov A M, Mashkova E S, Molchanov V A *Phys. Lett. A* **66** 129 (1978)
202. Mitrovic B C, O'Connor D J, Shen Y G *Surf. Rev. Lett.* **5** 599 (1998)
203. Bastasz R et al. *Surf. Sci.* **571** 31 (2004)
204. Sinel'nikov D N et al. "Analiz izotopov vodoroda na poverkhnosti vol'frama s pomoshch'yu spektroskopii malouglovogo ionnogo rasseyaniya" ("Analysis of hydrogen isotopes on a tungsten surface using small-angle ion scattering spectroscopy"), in *Problemy Termoyadernoi Energetiki i Plazmennye Tekhnologii, Materialy III Mezhdunarod. Konf., 16–21 Oktyabrya 2023, Tarusa* (Problems of Fusion Energy and Plasma Technologies, Proc. of the 3rd Intern. Conf. October 16–21, 2023, Tarusa) (Moscow: Izd. Dom MEI, 2023) p. 100; https://www.elibrary.ru/item.asp2id = 54792663
205. Spectroscopy vs. Spectrometry, Verichek Technical Services, https://verichek.net/spectroscopy-vs-spectrometry.html
206. https://goldbook.iupac.org/terms/view/S05848
207. Babenko P Yu et al. *Tech. Phys. Lett.* **48** (7) 50 (2022); *Pis'ma Zh. Tekh. Fiz.* **48** (14) 10 (2022)
208. Verbeek H, Eckstein W, Bhattacharya R S *J. Appl. Phys.* **51** 1783 (1980)
209. Babenko P Yu, Mikhailov V S, Zinoviev A N *JETP Lett.* **117** 725 (2023); *Pis'ma Zh. Eksp. Teor. Fiz.* **117** 723 (2023)
210. Kittel C *Introduction to Solid State Physics* 8th ed. (Hoboken, NJ: J. Wiley and Sons, 2005); Translated into Russian from 5th English Ed.: *Vvedenie v Fiziku Tverdogo Tela* (Moscow: Nauka, 1978)
211. Rabalais J W *Surf. Sci.* **299–300** 219 (1994)
212. Masson F, Rabalais J W *Chem. Phys. Lett.* **179** 63 (1991)
213. Shi M, Wang Y, Rabalais J W *Phys. Rev. B* **48** 1689 (1993)
214. Bolotin I L et al. *Surf. Sci.* **472** 205 (2001)
215. Rabalais J W *Analytical Chem.* **73** 206A (2001)
216. Bykov V, Houssiau L, Rabalais J W *J. Phys. Chem. B* **104** 6340 (2000)
217. Bolotin I L, Houssiau L, Rabalais J W *J. Chem. Phys.* **112** 7181 (2000)
218. Houssiau L et al. *J. Chem. Phys.* **110** 8139 (1999)
219. Moisson J M, Bensoussan M *J. Vac. Sci. Technol.* **21** 315 (1982)
220. Aono M et al. *Nucl. Instrum. Meth. Phys. Res B* **37–38** 264 (1989)
221. Aono M, Katayama M "Impact collision ion scattering spectroscopy," in *Compendium of Surface and Interface Analysis* (Singapore: Springer, 2018) p. 275, DOI:10.1007/978-981-10-6156-1_45
222. Miret-Artés S, Pollak E *Surf. Sci. Rep.* **67** 161 (2012)
223. Yurasova V E, Karpuzov D S *Fiz. Tverd. Tela* **9** 2508 (1967)
224. Tiwald P et al. *Phys. Rev. B* **82** 125453 (2010)
225. Babenko P Yu et al. *Nucl. Instrum. Meth. Phys. Res. B* **406** 460 (2017)
226. Babenko P Yu et al. *J. Exp. Theor. Phys.* **128** 523 (2019); *Zh. Eksp. Teor. Fiz.* **155** 612 (2019)
227. Hulpke E, Mann K *Surf. Sci.* **133** 171 (1983)
228. Tenner A D et al. *Surf. Sci.* **172** 121 (1986)
229. Tongson L L, Cooper C B *Surf. Sci.* **52** 263 (1975)
230. Wallington M J *J. Phys. E* **4** 1 (1971) DOI:10.1088/0022-3735/4/1/001
231. Aristarkhova A A et al. *Pis'ma Zh. Tekh. Fiz.* **17** (4) 81 (1991)
232. Volkov S S, Putilin I K *Izv. Ross. Akad. Nauk. Ser. Fiz.* **62** 2026 (1998)
233. Gordon M J, Giapis K P *Rev. Sci. Instrum.* **76** 083302 (2005)
234. Tolstogouzov A, Daolio S, Pagura C *Nucl. Instrum. Meth. Phys. Res. B* **183** 116 (2001)
235. Gordon M J, Mace J, Giapis K P *Phys. Rev A* **72** 012904 (2005)
236. Kutana A, Gordon M J, Giapis K P *Nucl. Instrum. Meth. Phys. Res. B* **248** 16 (2006)
237. Rezayat T, Shukla A K *Nucl. Instrum. Meth. Phys. Res. B* **264** 400 (2007)
238. Johnson P R, Sosolik C E *Comput. Phys. Commun.* **280** 108479 (2022)
239. Yang M C et al. *Surf. Sci.* **357–358** 595 (1996)
240. Dahl E B et al. *Nucl. Instrum. Meth. Phys. Res. B* **125** 237 (1997)
241. Veksler V I *Sov. Phys. JETP* **22** 65 (1966); *Zh. Eksp. Teor. Fiz.* **49** 90 (1965)
242. Ferleger V Kh, Wojciechowski I A *Nucl. Instrum. Meth. Phys. Res. B* **164–165** 641 (2000)
243. Smith R (Ed.) *Atomic and Ion Collisions in Solids and at Surfaces: Theory Simulation and Applications* (Cambridge: Cambridge Univ. Press, 1997)
244. Gubin S P *Khimiya Klasterov: Osnovy Klassifikatsii i Stroenie* (Cluster Chemistry: Basic Classification and Structure) (Moscow: Nauka, 1987)
245. Aristarkhova A A et al. *Poverkhnost'. Rentgen., Sinkhrotron., Neitron. Issled.* (7) 27 (2006)
246. Bundaleski N et al. *Nucl. Instrum. Meth. Phys. Res. B* **256** 86 (2007)
247. Grundner M, Heiland W, Taglauer E *Appl. Phys.* **4** 243 (1974)

248. Bernheim M, Slodzian G *Nucl. Instrum. Meth.* **132** 615 (1976)
249. Schultz J A, Kumar R, Rabalais J W *Chem. Phys. Lett.* **100** 214 (1983)
250. Tolstoguzov A B et al. *Tech. Phys. Lett.* **42** 915 (2016); *Pis'ma Zh. Tekh. Fiz.* **42** (17) 70 (2016)
251. Wittmaack K *Phys. Rev. B* **56** R5701 (1997)
252. Wittmaack K *J. Vac. Sci. Technol. A* **15** 2557 (1997)
253. Franzreb K et al. *Surf. Interface Anal.* **26** 597 (1998)
254. Franzreb K, Williams P *Appl. Surf. Sci.* **203–204** 98 (2003)
255. Products. Hiden Analytical, https://www.hidenanalytical.com/products/
256. Tolstogouzov A et al. *Int. J. Mass Spectrom.* **214** 327 (2002)
257. Tolstoguzov A B, Gusev S I, Fu D J *Tech. Phys. Lett.* **49** (1) 32 (2023); *Pis'ma Zh. Tekh. Fiz.* **49** (1) 35 (2023)
258. Daolio S, Pagura C, Tolstogouzov A *Appl. Surf. Sci.* **222** 166 (2004)
259. De Ruitz M *Monete a Venezia nel tardo Medioevo. Un ritorno alle fonti* (Treviso: Canova, 2001)
260. Tolstogouzov A B, Greenwood C L *Poverkhnost'. Rentgen., Sinkhrotron., Neitron. Issled.* (12) 33 (2002)
261. Bardi U et al. *Appl. Surf. Sci.* **252** 7373 (2006)
262. Tondare V N *J. Vac. Sci. Technol. A* **23** 1498 (2005)
263. Hill R, Notte J, Ward B *Phys. Proced.* **1** 135 (2008)
264. Sijbrandij S et al. *J. Vac. Sci. Technol. B* **26** 2103 (2008)
265. Sijbrandij S et al. *J. Vac. Sci. Technol. B* **28** 73 (2010)
266. Klingner N et al. *Ultramicroscopy* **162** 91 (2016)
267. Newbury D E *Scanning* **27** 227 (2005)
268. Grachev S Y et al. *Nucl. Instrum. Meth. Phys. Res. B* **219–220** 593 (2004)
269. Wang Y et al. *J. Nucl. Mater.* **593** 154975 (2024)
270. Efimov N et al. *Nucl. Instrum. Meth. Phys. Res. B* **546** 165177 (2024)
271. Efimov N et al. *Nucl. Instrum. Meth. Phys. Res. B* **567** 165823 (2025)